BLDC Motor Power Control Techniques Appraisal: Novel current control Technique

Master's Thesis

work by

Michael Thomas Ratcliffe

February, 2014

Lancaster University

Faculty of Science and Technology

Engineering Department

Signed Declaration on the Submission of a Project

I declare that this project is my own work and has not been submitted in substantially the same form towards the award of a degree or other qualificatory work, and affirm that acknowledgement has been made to assistance given and that all major sources have been appropriately referenced.

Signed: ……

Date: ……

ABSTRACT

Abstract—**This paper details current state of the art with respect to digital motor commutation and power control techniques, illustrates the distinct advantages and disadvantages of each technique and goes on to propose a novel current control technique aimed at increasing efficiency at high speed part load conditions, and goes on to evaluate the technique by simulation.**

Keywords- BLDC motor, trapeziodal comutation, sinusoidal comutation, field oriented control, digital motor, PMSM

Acknowledgments

The author would like to acknowledge the financial support provided by the Sir John Fisher Foundation, who's funding has allowed this research to take place, He would also like to thank the IMechE for kindly contributing towards his undergraduate degree.

Whilst acknowledging the input from the engineering department in general he would like to show extra gratitude towards the following people for their time and patience: Dr. Kelum Gamage (project supervisor), Dr James Taylor and Bob Makin of the faculty for donating their time, energy and rare ability to explain complex topics in plain language.

Contents

List of Figures

List of Tables

Symbols

E	Total back emf
e	Phase emf
Fr	Friction constant
I	Current
J	Inertia
Kp	Feed back loop proportional constant
Ki	Feedback loop Integral constant
Kd	Feedback loop Derivative constant
Kv	BEMF constant
L	Inductance
N	Magnetic south pole
P	Magnetic pole pairs
Q	Electronic switch
R	Resistance
S	Magnetic south pole
t	Time
T	Torque
V	Voltage
Θ	Angular position
ω	Angular speed

Subscripts

1	Phase a High leg
2	Phase b High leg
3	Phase cHigh leg
4	Phase a Low leg
5	Phase b Low leg
6	Phase c Low leg
a	Phase a
b	Phase b
c	Phase c
batt	Battery (source) voltage
e	electrical
fall	Fall time for mosfet
L	load
m	mechanical
n	Central node
on	Total turn on time
off	Total switch off time
r	Rotor
rise	Rise time for mosfet

Abbreviations

BLDC	Brushless DC Motor
DC	Direct current
CA	Conduction angle
Emf	Electro magnetic force
ESC	Electronic speed controller
Mech	Mechanical
PAM	Pulse amplitude modulation
PWM	Pulse width modulation
Rpm	Revolutions per minute

Digital media

The CD below contains information relating to this report, a soft copy of thesis work, appendices and two copies of simulation software. One version models the ESC as ideal and as such neglects the losses associated with it. This speeds up simulation time and is useful in work relating to control loop tuning. The second is a full simulator taking into account the losses associated with the ESC, giving greater accuracy but at the expense of computational power and time.

Chapter 1: Introduction

Recent years have seen the widespread adoption of digital motors as the power house behind many power systems due to their relatively high efficiency and controllability. A good example of this is shown in the maritime/shipping industry, where many of the power systems within the ship are moving towards electrical power systems. Multiple respectable articles speculate that in the near future, ships will operate purely from electrical drive systems.

In a more general sense, digital motors are being used in thousands of applications across many sectors , to add a sense of magnitude to this, studies (see **Error! Not a valid bookmark self-reference.**) have shown that In 2007 BLDC motors accounted for 23% of American electric motor power usage (1), of which electric motors are accountable for 46% of electrical power usage overall (2) (see Figure 2) meaning that BLDC motors are accountable for around 11% of all power usage. As it can be seen, any advancement in digital motor control that leads to higher efficiency will result in a massive reduction in waste energy worldwide.

The BLDC motor boasts higher efficiency when compared to traditional brushed motors; however like any real system they still have losses. One cause of loss that is often ignored the losses associated with the controller with a large portion of this loss being related to the switching losses.

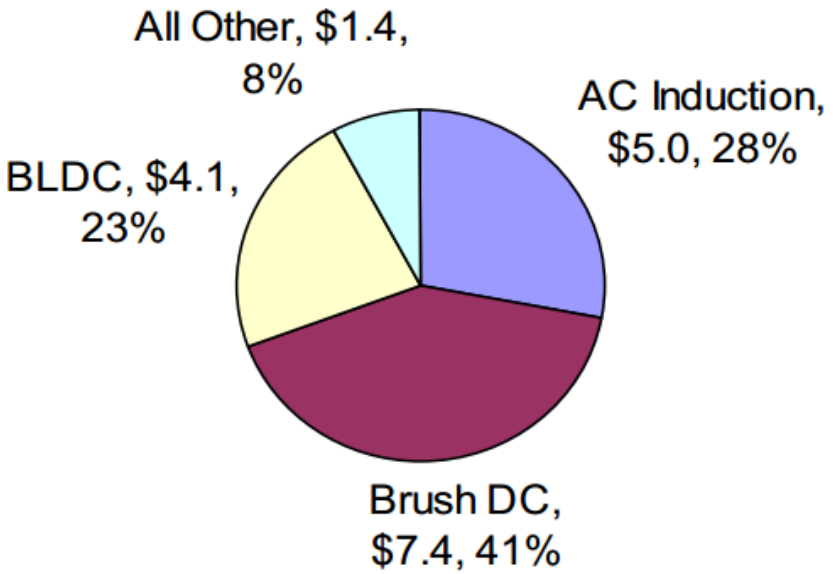

Figure 1 – 2007 Electric Motor Consumption in North America Total $18B (1)

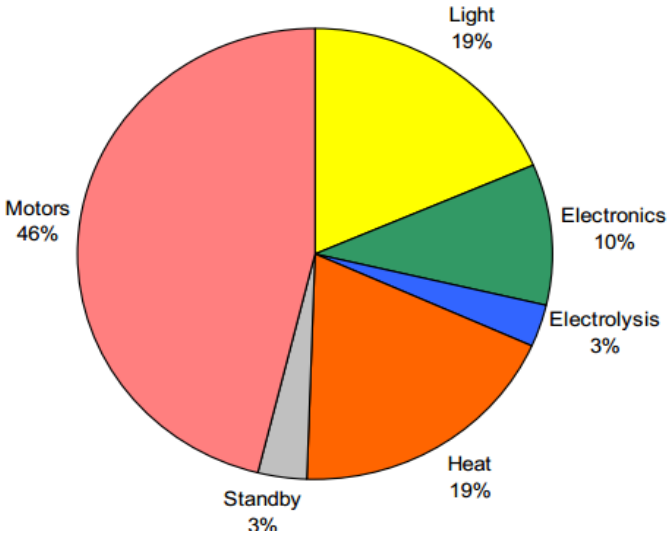

Figure 2- Estimated share of global electricity demand by end-use (2006) (2)

When the system is running at full power and thus at a duty cycle of 100% switching losses are proportional to the commutation frequency of the motor. However, when this duty cycles is any value below unity, the switching losses are proportional to the PWM frequency, which is often magnitudes greater than the commutation frequency.

This thesis proposes and tests a novel power control technique that is aimed at reducing the switching losses by bringing the frequency of PWM power control signal down to that of the commutation frequency for much lower duty cycles.

The outline of each chapter is as follows:

Note: Versions of chapters one to six have been published in the IEEE 2013 Power Engineering, Energy and Electrical Drives (POWERENG), 2013 Fourth International Conference journal. This has been included at the end of the thesis in the form of appendix F.

- **Chapter 2**

  Presents digital motors in general and goes on to detail how BLDC motors differ from other types of permanent magnet synchronous machines.

- **Chapter 3**

  Describes the commutation process of BLDC motors and gives examples of the current state of the art.

- **Chapter 4**

  Presents the types of power control techniques most popularly used in respect to BLDC motors, concluding with a summary about their use in applications and factors leading the choice of a suitable technique based on application.

- **Chapter 5**

  Introduces the proposed power control technique, detailing the theory behind its operation and outlining potential pro's and cons of its use.

- **Chapter 6**

  Presents potential ways to simulate a BLDC motors operation using Matlab/Simulink software package and goes on to detail the reasoning as to why the chosen method was finally selected.

- **Chapter 7**

  This chapter explains the process of implementing a simulator based on the conclusions drawn from the previous chapter.

- **Chapter 8**

  Compares the operation and results of the simulator designed in the previous chapter to other proven simulators from published literature, the simulator operates as expected and produces results correlating with said literature.

- **Chapter 9**

  Presents the results of the simulator for traditional techniques alongside the proposed technique in areas of interest with respect to system operation.

- **Conclusions**

  This final section draws conclusions about the techniques suitability in real world application referring to results from the previous section.

Chapter 2: BLDC Motor Characteristics

With the development of semiconductor technology, a new age for motors has begun, the age of the digitally commutated motor.

2.1 Advantages of Digital Motors

Digital motors can be split into two main categories, synchronous and asynchronous. This thesis is based around BLDC motors. BLDC motors are a form of synchronous motor, meaning the magnetic field generated by the stator and the magnetic field of the rotor rotate at the same frequency.

Digital motors can have many mechanical layouts, for example the rotor can be internal or external and the number of phases can vary from one upwards (3), with three-phase motors being the most popular and widely adopted kind.

Digital synchronous motors have the following benefits when compared to mechanically commutated motors (4) (5)[commutation is covered in the following chapter]:

- Long operating Life
- High dynamic response
- High efficiency
- Better speed vs torque characteristics
- Noiseless operation
- Higher speed range
- High power to weight ratio

2.2 Types of Synchronous Digital Motors

Digital synchronous motors can be categorised into two main groups based upon the shape of their Back Electromotive Force (BEMF) (6)(7). One produces a trapeziodal BEMF and is reffered to as a Brushles DC Motor (BLDC), whilst the other producesa sinusoidal BEMF and is commonly refered to as a permanent Magnet Synchronous Motor (PMSM).

Figure 3 shows the idealised BEMF shapes of the BLDC and PMSM, mechanical limitation in the manufaturing process of the windings however produce less than perfect BEMF waveforms.

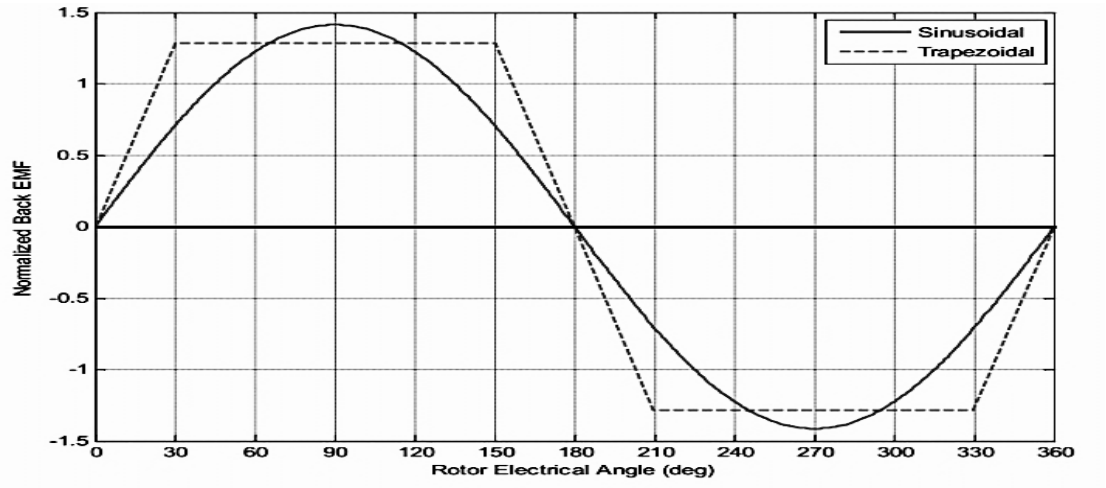

Figure 3- BLDC vs. PMSM idealized BEMF for one phase (6)

The operation and characteristics of the BLDC motor are very similar to that of a brushed DC motor, but the lack of brushes reduces the frictional losses increases the operating speed and allows the use of high level control. Due to the nature of a BLDC motor it is necessary to perform the commutation via a dedicated digital driving circuit. There are many types of BLDC driver circuits, the majority of which are bipolar (both high and low side semiconductors, aka H-bridge) 3-phase drivers, see Figure 4.

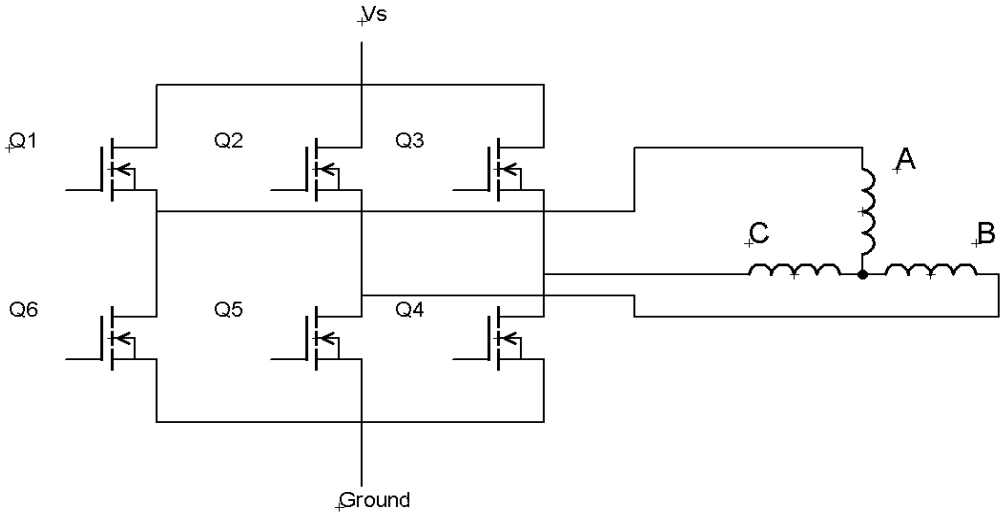

Figure 4 - Three phase inverter and motor

Chapter 3: Commutation

Commutation refers to the process of creating a rotating magnetic field in the stator of the motor in the desired direction. There are three main ways to achieve commutation (8) (9), which all rely on the manipulation of the H-bridge shown in Figure 4. Each one carries a distinct set of advantages and disadvantages that will be discussed in this chapter.

3.2 Trapezoidal

This is the simplest form of commutation as it uses the trapezoidal technique, meaning only two of the three phases are ever simultaneously powered. During one electrical revolution, six commutation steps take place as current can flow both ways within the inductors (Figure 5), giving rise to six stator flux vectors as shown in Figure 6.

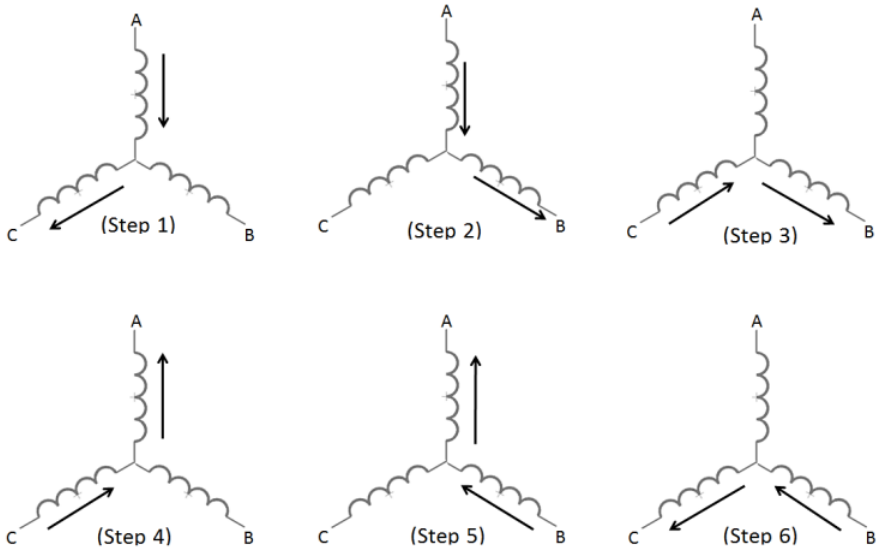

Figure 5- Current flow to produce rotating magnetic field

In order for the controller to switch to the next commutation step at the correct time the position of the rotor must be known. This can be achieved once rotation has commenced by sensing the BEMF of the unused phase, or from a standstill by reading binary outputs from just three sensors separated by 120° electrical, commonly latching magnetic hall sensors are used due to their robustness and relative cheap cost (10)(11). Once the rotor position is known it can be compared to lookup tables relating to the desired operating direction.

When trapezoidal commutation is used to drive a BLDC motor it results in constant torque due to the driving waveform (Figure 3) matching the BEMF (12) (12)waveform of the motor. In this case, current cannot penetrate a motor phase instantly leading to torque ripples every commutation step, six times per electrical revolution (Figure 7). However many applications are immune to a certain amount of torque ripple and it has little to no effect on the motors performance.

The same cannot be said when driving a PMSM with the Trapezoidal technique, as torque ripple is produced from the miss match between driving and BEMF waveforms causing less than optimal flux interaction angle. This coupled with the ripple from the commutation step produces relatively high torque ripple as shown in Figure 8.

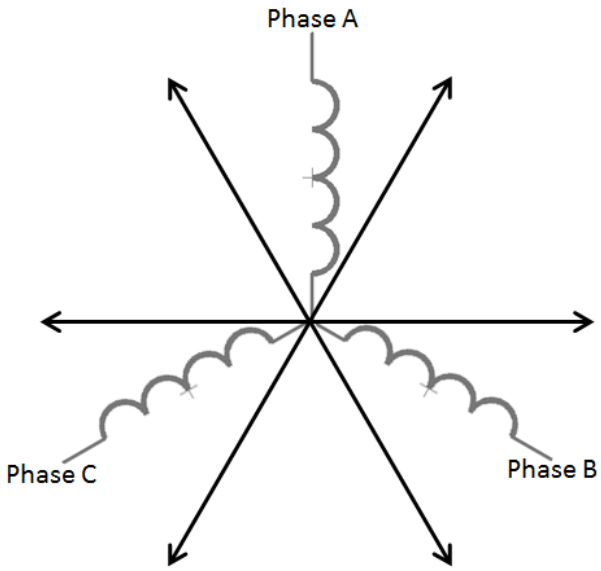

Figure 6- Stator flux vector locations, ABC =rough position sensors

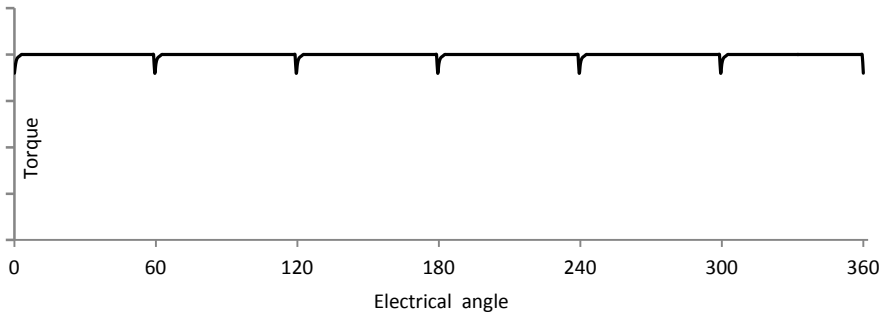

Figure 7- Trapezoidal driven BLDC torque ripple

3.3 Sinusoidal

Sinusoidal commutation attempts to create a rotating field that can constantly keep the flux vector interaction angle at ninety degrees to optimize efficiency and reduce torque ripple. It achieves this by manipulating all three phases simultaneously to produce three sine waves of the desired frequency each 120^{o} apart. This is the sinusoidal shape of this driving waveform that produces smooth ripple free torque (10). In order to achieve a smooth sinusoidal wave, the rotor position is required to a much greater accuracy in comparison to trapezoidal techniques. This is achieved by a position sensor with a resolution much larger than the commutation step. The output from the sensor is then used to compute the desired PWM ratio at that point to create a sinusoidal waveform. If a sinusoidal waveform is used to drive a BLDC motor, the torque will have ripples similar to those of a PMSM driven by a trapezoidal waveform (Figure 8), the only difference being additional ripples introduced from the commutation as it is no longer discreet steps.

Simple sinusoidal commutation does however have some drawbacks. The feedback system that controls the current to the phases tends to fail at high operating speeds - as the speed increases the current loop controllers have to track a sinusoidal signal of high frequency, and the proportional-integral (P-I) controllers used have a limited gain and frequency response. This results in lag and gain errors in the motor currents, as the slew rate of the feedback system isn't fast enough.

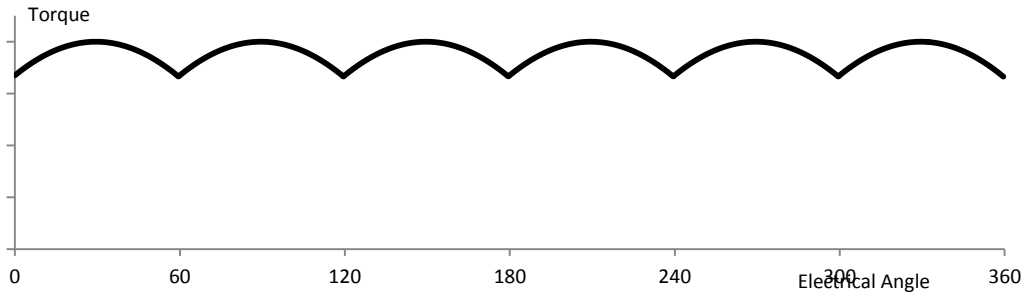

Figure 8- PMSM trapezoidal driven

3.4 Field Oriented Control [FOC]

FOC is an advanced type of sinusoidal driving technique, with the difference being the control system to generate the driving waveforms is relatively complex and as such is considered a high end commutation technique due to its large processing requirements.

An advantage of this is that it offers high efficiency over a wide operating range whilst giving precise control over torque and speed.

This is achieved by moving the feedback loop from a time and speed dependent system into a two co-ordinate time invariant system. Removing the previous bandwidth limitations of the controller, as it is now seen as a DC system from the controller's point of view, with separate processors taking care of transforming between the two reference systems.

Implemented by utilising two transforms, the first step is performing a Clarke transform (13), which gives a two variable representation of the three phase. This is followed by performing a Park transform on the new two variable representation to move it from a stationary reference frame to a rotating, proceeding to use these new DC values to compute the error signal for the PI controller. Taking the flux positions of the rotor and stator and transforms them into easy to compute DC components Iq(torque) and Id(magnetising). To achieve maximum efficiency, two PI control loops are used to equate Id to zero and Iq equal to the desired current to control torque.

3.5 Commutation Summary

As previously mentioned, each commutation technique has associated benefits and drawbacks and there is no perfect solution to every problem. Table 1 outlines the major advantages and disadvantages of each which should be considered when selecting a commutation technique, assuming the commutation technique is being applied to the correct motor.

Technique	Trapezoidal	Sinusoidal	FOC
Power density	High	Low	Low
Start-up power	High starting torque, but lots of ripple	Lower but smooth starting torque	Lower starting torque
Power delivery	High torque ripple	Smooth	Smooth
Speed control	Excellent	Excellent	Excellent
High speed performance	Good	Poor	Excellent
Position sensing	Hall (simple)	Encoder/resolver	Encoder and current sensor
Controller complexity	Low	Medium	High

Table 1 Commutation summary

Chapter 4: Power Control

The previous section discussed the method in which the rotating field is generated. To control torque it is necessary to control the current input into the motor because the two are directly linked(14). There are three methods commonly implemented to achieve current control for BLDC motors that are going to be discussed in this chapter.

4.1 Pulse Amplitude Modulation [PAM]

PAM can be used to control the current for all three of the aforementioned commutation techniques, as the applied voltage across the motor is reduced by controlling the bus voltage. This is one of the simplest methods of current control. Figure 9 shows one common method of implementation when drawing power from a DC source: a semiconducting device is placed between the three phase H-bridge and power source. The duty cycle applied to this device dictates the current supplied to the motor with the H-Bridge being responsible for only commutation.

(14)

Figure 9 Dc Bus Bar control Aka PAM

4.2 Pulse Width Modulation [PWM]

The motor controller is connected to the full rated bus voltage and differs from other methods as it controls the current through the motor by altering the duty cycle driving the three phase H-bridge. There are two types of switching strategies when considering PWM control - hard chopping, where both the high and low switches are controlled by PWM and soft chopping, in which the lower switches continuously conduct and only the top fed with PWM (15), unless otherwise stated Hard Chopping PWM is used in this document.

Hard chopping has the advantage of easier control as it only needs to handle three input signals and relies on simple logic components to ensure that a phase is never shorted. However, this method introduces the disadvantage of increased torque ripple and increased switching losses.

In comparison, soft chopping requires six input signals to independently control each switch. This increases the level of control over the system by reducing torque ripple and switching losses by a factor of two when compared to hard chopping, due to the lower switches constantly conducing (Figure 10).

PWM is already implemented in sinusoidal and FOC commutation to generate the three phase input waveforms in order to control the current going to the motor the ratio of pulses remains constant but the average duty cycle is reduced.

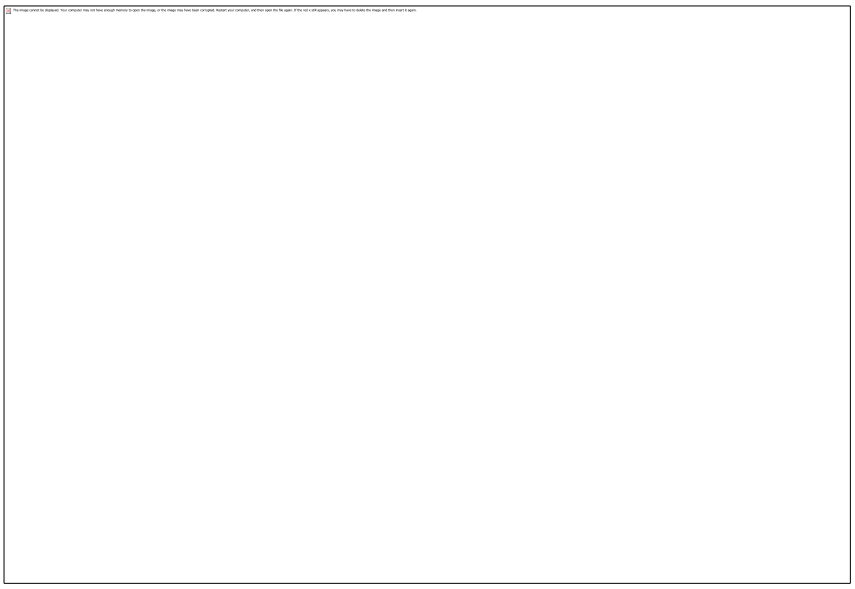

Figure 10 Soft chopping PWM for one electrical cycle, 50 percent duty cycle

4.3 Hysteresis Current Control [HCC]

HCC monitors the current through the motor and forces it to stay within a predefined band, which indirectly controls the voltage. Unlike the previous two strategies the on/off frequency is not a fixed value, rather it varies depending on the load conditions. This variable switching frequency can result in switching harmonics that appear over a wide frequency making the filtering relatively difficult. HCC however does have advantages, as the switching frequency is generally less, which results in lower switching losses for the controller. This means it is protected from over current and damaging the motor or controller if the rotor was to become locked [this will be discussed in later chapters]

Chapter 5: Proposed Novel Technique, Conduction Angle Control [CA]

The proposed novel power control technique is aimed at increasing the part load efficiency of BLDC power systems of high inertia or systems running at high speed. By centring the driving current around the optimum flux interaction point and bringing the PWM frequency down to that of the commutation frequency to reduce switching losses within the system, without adding any extra components or physical parts to the system, that is it will be entirely software based.

5.1 Technique Operation

Consider one commutation step for traditional trapezoidal commutation, using PWM to limit current flow (Figure 11). Each time one of the pulses rises/falls the switching device acts as a variable resistor resulting in hefty copper losses, independent of duty cycle. The proposed technique will replace the many voltage inputs by one prolonged input where the duty cycle is the ON time of the pulse relative to the time of the commutation step (Figure 12), effectively controlling the angle of conduction. Reducing the switching losses and increasing the controller efficiency at the expense of torque ripple.

Many research projects have been aimed at reducing the torque ripple produced by commutation (16)(17), to reduce the vibrations in the motor and reduce the audible noise. However for many applications that are high speed or high inertia the weight of the system smooth's any minor ripples out before it has a major effects on the system as a whole. The torque ripple associated with the proposed control technique could potentially fall within this safe range of ripple torque.

There are several limitations to this technique, it cannot be used at low speeds or low duty cycles, these situations will be dealt with by using the traditional PWM control, the transition between techniques will be handled by the controller without the addition of a small amount of code.

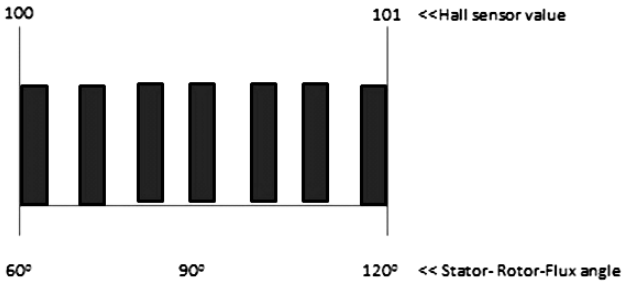

Figure 11 PWM driving signal, single commutation step

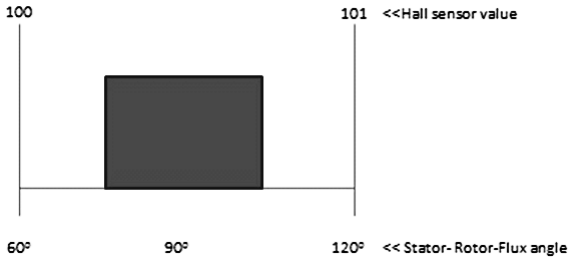

Figure 12 Proposed CA technique driving signal

Other potential benefits of this technique include increased immunity to inefficient flux interaction angles brought about by flux skewing, driving waveform lag and added security from damage in locked rotor situation due to the pulse length being time dependent and not reliant on input from position sensors.

Chapter 6: Simulation Methods

To verify the concept behind the CA-hybrid current control technique and conclude the conditions under which it can efficiently operate, simulation will be carried out. They will be aimed at investigating the commutation techniques effect of efficiency and operating characteristics, the main characteristic of interest being speed fluctuation.

Due to the heavy research around the area of BLDC motors, many papers cover the simulation of BLDC motors they all share the same in common, that is the use of a simulation package like MATLAB Simulink to simulate the operation. There are many ways to simulate the operation but they can be slip into two main categories, one set uses the manipulation of underlying governing equation for each part of the system while the other uses advanced tool boxes to generate the results.

The benefits and draw backs of each method will be discussed in this chapter.

6.1 Tool Box Methods

One major drawback about using this type of simulation is that the toolbox currently runs the simulation assuming the semiconductors are ideal (18) that is it doesn't take into account switching losses; this is a major drawback when the area of interest is switching losses.

6.2 Manipulation of Governing Equations

The techniques that fall into this category all rely on traditional simulation techniques of building a mathematical model representation of the system by manipulation of the equations governing each part of the system, this process is shown below.

Assuming that the driving currents/waveforms from the controller are of the same shape and in phase with the BEMF of the motor it is possible to relate the torque produced by the motor to the total current input of the motor:

$$\tau_e = [e_a i_a + e_b i_b + e_c i_c]*[1/\omega_r] \quad [1]$$

Where τ_e is the electrical torque, e_a is the BEMF of phase, i_a is the current flowing through phase-a and ω_r is the angular velocity of the rotor.

The interaction of τ_e with the load torque $\tau_L$will allow simulation of how the motor speeds up from a standstill, reacts to changes in load conditions and the speed change of the motor arising from torque ripple by manipulation of equation-2 (19) (19).

$$\tau_e = \tau_L + J\left(\frac{d\omega r}{dt}\right) + Fr\omega_r \quad [2]$$

J- Moment of inertia Fr-Friction

With very few assumptions it is possible to accurately model a BLDC motors reaction to driving inputs ,Figure 13 shows the equivalent circuit diagram for the stator of a star wound motor it takes into account the resistance (R), inductance (L) and BEMF (e) of each phase that will be used to build the equations needed to model the motor. In order to calculate the electrical torque produced by the motor it is necessary to derive the current flowing through the windings for use in equation-1.

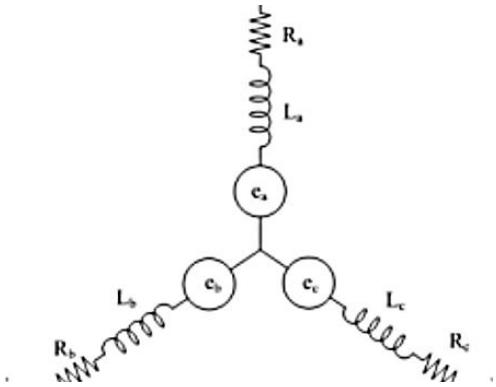

Figure 13 Equivalent stator circuit

Calculating the current flowing through the motor is accompanied by extra complexity as the current is a function of winding resistance, inductance and BEMF, this is best described by the general motor equation (19)(20).

$$\begin{bmatrix} Va \\ Vb \\ Vc \end{bmatrix} = \begin{bmatrix} Ra & 0 & 0 \\ 0 & Rb & 0 \\ 0 & 0 & Rc \end{bmatrix} \begin{bmatrix} ia \\ ib \\ ic \end{bmatrix} + \begin{bmatrix} Laa & Lab & Lac \\ Lba & Lbb & Lbc \\ Lca & Lcb & Lcc \end{bmatrix} \frac{d}{dt} \begin{bmatrix} ia \\ ib \\ ic \end{bmatrix} + \begin{bmatrix} ea \\ eb \\ ec \end{bmatrix} \quad [3]$$

Where R is resistance, L inductance, i current and e BEMF the subscripts show the relative phase. With the assumption that all three phases are balanced and if there is no change in the rotor reluctance with angle because of a non-salient rotor, this can be simplified to:

$$\begin{bmatrix} Va \\ Vb \\ Vc \end{bmatrix} = \begin{bmatrix} R & 0 & 0 \\ 0 & R & 0 \\ 0 & 0 & R \end{bmatrix} \begin{bmatrix} ia \\ ib \\ ic \end{bmatrix} + \begin{bmatrix} Laa & 0 & 0 \\ 0 & Lbb & 0 \\ 0 & 0 & Lcc \end{bmatrix} \frac{d}{dt} \begin{bmatrix} ia \\ ib \\ ic \end{bmatrix} + \begin{bmatrix} ea \\ eb \\ ec \end{bmatrix} \quad [4]$$

This matrix can then be manipulated to evaluate the current across each phase dependent upon the input voltage from the controller, and the calculated currents can be substituted back into equation 1, to calculate the instantaneous torque at that moment.

The next step will involve increasing the complexity of the simulation to take into account the losses from the controller, there are two main losses arising from the three phase inverter conduction losses (copper losses) and switching losses.

Assuming that both the high and low side of the three phase inverter use the same semiconductors it is possible to add their resistance to the corresponding phase resistance in equation-4, leading to equation-5:

$$\begin{bmatrix} Va \\ Vb \\ Vc \end{bmatrix} = \begin{bmatrix} Rt & 0 & 0 \\ 0 & Rt & 0 \\ 0 & 0 & Rt \end{bmatrix} \begin{bmatrix} ia \\ ib \\ ic \end{bmatrix} + \begin{bmatrix} Laa & 0 & 0 \\ 0 & Lbb & 0 \\ 0 & 0 & Lcc \end{bmatrix} \frac{d}{dt} \begin{bmatrix} ia \\ ib \\ ic \end{bmatrix} + \begin{bmatrix} ea \\ eb \\ ec \end{bmatrix} \quad [5]$$

Where R_t is the addition of the motor phase resistance and the controller resistance.

The average magnitude E of the BEMF of a motor is relatively easy to calculate due to it being linearly related to speed as:

$$E = K_b \omega_r \quad [6]$$

Where K_b is a constant, the value is determined by the strength of the permanent magnets in the rotor and density of windings in the stator. Any respectable BLDC motor manufacturer will include this value within the motors data sheet.

An ideal BLDC motor has a trapezoidal BEMF per phase; the BEMF can be expressed as below (19):

$$\begin{aligned} e_a &= E && when \quad 0^o<\theta_r<120^o \\ e_a &= \left(\frac{6E}{n}\right)(n - \theta r) - E && when \quad 120^o<\theta_r<180^o \\ e_a &= -E && when \quad 180^o<\theta_r<300^o \\ e_a &= \left(\frac{6E}{n}\right)(\theta r - n) - E && when \quad 300^o<\theta_r<360^o \end{aligned} \quad [7]$$

Where θ_r represent the rotor position in electrical degrees.

The combination of the above equations[1,2,5] provide enough information to efficiently model a BLDC motor, the actual modeling of the motor in the Simulink environment can be undertaken in one of three ways as discussed below:

6.21 Block Diagram

Block diagram, this is a visual method of describing a system, Figure 14 shows the block diagram representation of the relationship described in equation(2), it has the benefit of being able to set initial conditions like operating speed and torque. Any input variable or internal variable can also be measured using this method.

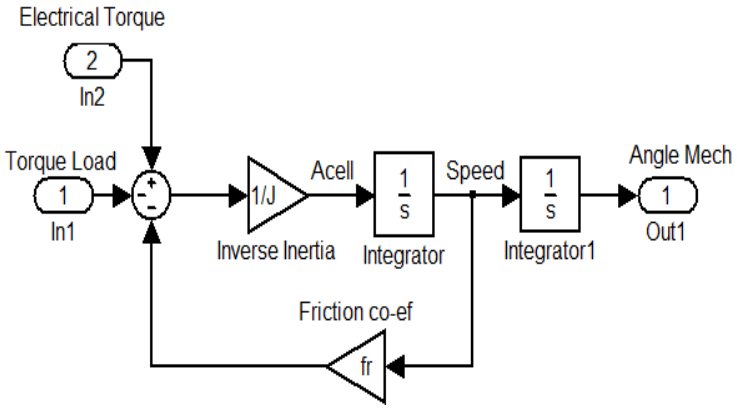

Figure 14 Block diagram representation of equation-2

6.22 Transfer Function

Transfer function, the system can be condensed into a transfer function to reduce the size of the model, this however does not allow the setting of initial conditions or the measuring of internal variables to the same extent as block diagram.

6.23 State space

State space model, the equations (1,2,5) are arranged into matrices of the standard state space form. This has the added benefit of reducing the size of the model whilst retaining the ability to set initial conditions, but is a bit of a black box approach stopping the measurement of internal variables.

6.3 Adopted Simulation Technique

The manipulation of governing equations approach was chosen mainly because it required a better understanding of the inner workings of the BLDC motor and the aim of this project was not only to expanded advance engineering technology but to also expand the authors own knowledge and skill base. It is possible to simulate the BLDC motor by use of the governing equations in multiple ways, Block diagram analysis was chosen as again it offers a great opportunity for truly understanding the operation and gives access to internal values not possible by other methods.

Chapter 7: Simulation Operation

The simulator is implemented as block diagram for the reasons discussed in the previous chapter. This chapter delves deeper and expands to show the block diagrams in detail, outlining any assumptions and the impact of these assumptions.

The whole system can be broken down into four main sub systems as shown in Figure 15. The electrical and mechanical subsystems are generic to every driving technique and only the Electronic Speed Controller ESC subsystem varies dependent upon the current control technique being studied.

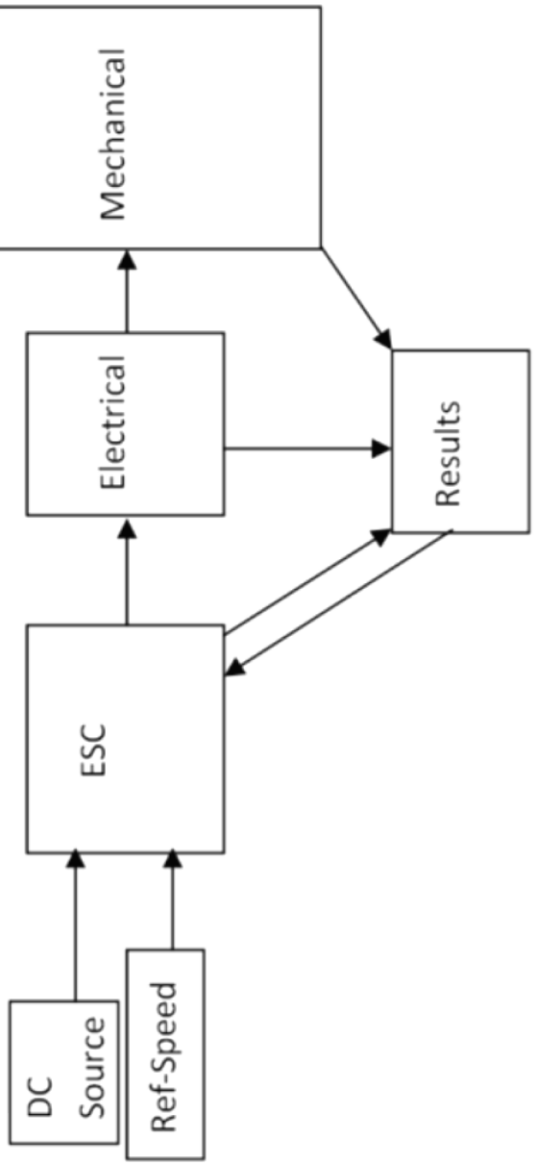

Figure 15 Simulator overview

To ease the process of running simulations and altering variables they are all defined before a simulation by the use of the command window - the variables for each section are detailed in tables 2 to 6. The power control technique must also be stated by assigning it a value of 1. All variables must be entered even if they are not related to the technique of interest, assigning them a random value will allow the operation of the simulator.

Simulation type	Reference	units
PWM	PWM	1=on 0=off
CAM	CA	1=run 0=off
PAM	PAM	1=on 0=off

Table 2- Simulation type arming signals

Input variable	reference	units	Notes
BEMF constant	Kv	Vs/rad	
Phase resistance	R	Ohms	Per phase
Phase inductance	L	Henries	Per phase

Table 3- Motor electrical parameters

Input variable	reference	units	notes
Inertia	J	Kg.m2	
Friction coefficient	Fr	Nms/rad	Related to mechanical speed
Number of poles	P	n/a	Total poles not pairs

Table 4- Motor mechanical parameters

Variable	Reference	units	notes
On resistance H-Bridge	H-Rt	Ohms	Per transistor
Switching time H-bridge	H-offon	Seconds	Total switching Time
PWM Frequency H-Bridge	H-Freq	Hz	
Source Voltage	Vs	Volts	DC only
PAM PWM Frequency	P-Freq	Hz	
On Resistance PAM	P-Rt	Ohms	For additional bus bar control
Switching Time total PAM	P-Toffon	seconds	

Table 5- ESC parameters

Input variable	reference	units	notes
Proportional constant	Kp	n/a	
Integral constant	Ki	n/a	

Table 6 Control values

7.1 assumptions and limitations

Real world systems are affected by many factors which can get extremely complex; however it is often found that they are largely dependent on a handful of the factors. This makes it possible to describe the operation of a system with relative ease by making certain assumptions. This can give very accurate and useful results provided the assumptions and their importance is understood, in order to compile the simulator many assumptions have been made, in example the modelling of PWM control was implemented upon the input voltage to the controller. This will deliver valid results for hard switching providing the PWM frequency is much greater than the commutation frequency, but would not provide a good representation for soft switching.

Table 7 details the major assumptions made and the limitations these can lead to.

Assumption	Limitation
Balanced Phases	Performance of Poorly made motors is not simulated accurately.
Ideal Trapezoidal BEMF	Only valid for BLDC motors, not ones with sinusoidal or heavily distorted BEMF patterns.
Loss calculation not valid for PWM value of unity	Switching losses are not valid for a duty cycle of unity
Stable operating temperature	Results only valid for motor that has reached steady operating temperature.
Feed back loop operates at 1KHz	Control system constants will vary depending upon actual loop frequency

Table 7 Simulation assumptions

7.2 Mechanical Portion

The mechanical system can be accurately described by a fist order differential equation. Equation 2 describes the mechanical portion of the system taking into account the losses arising from friction within the system and any useful power taken from said system; it is then possible to simulate the effect of the remaining power on the system by taking into account the systems inertia.

This equation has been translated into a block diagram [Figure 16].

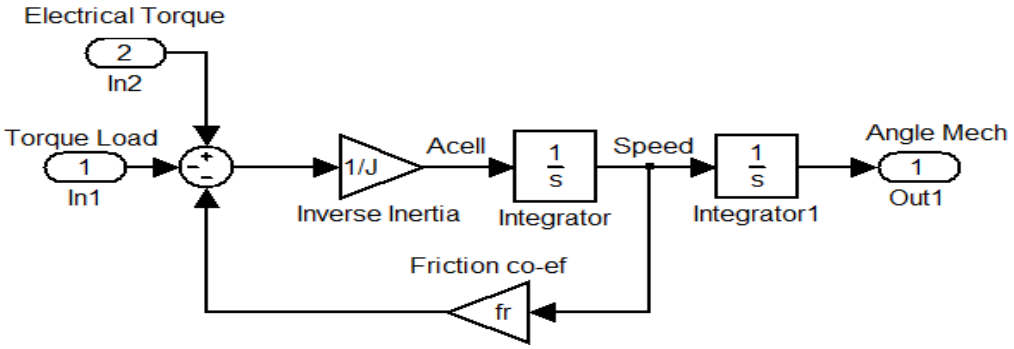

Figure 16 Mechanical system block diagram

7.3 Electrical Portion

This subsystem is a model representation of the electrical portion of the motor. Equation 5 forms the base of this block calculating an estimate for the current flowing within each winding taking into account the resistance, inductance and BEMF of each phase. For the block diagram representation of Equation 5 see Figure 17.

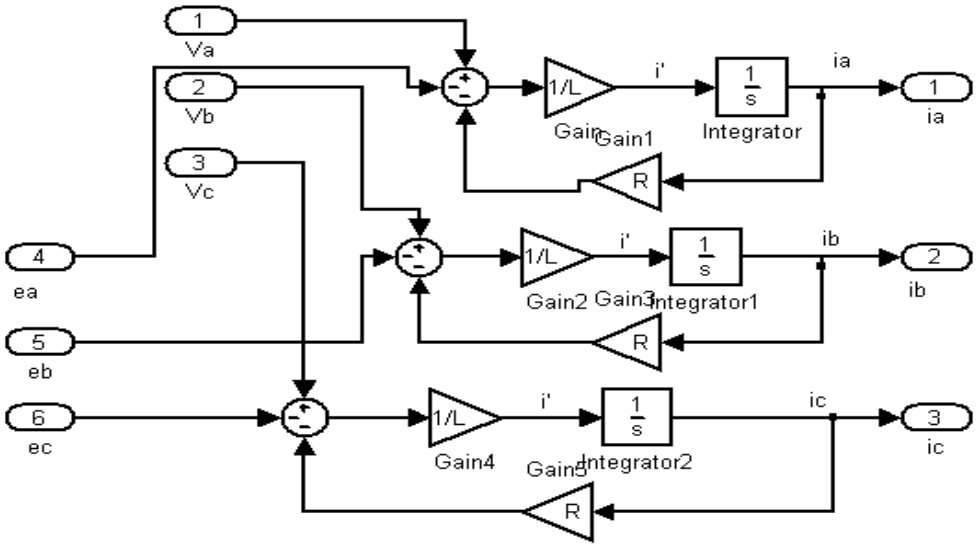

Figure 17 Current estimator

In order to calculate the current it is necessary to first know the voltage input into the windings and know the BEMF for each phase. The driving voltages will be generated by the ESC and will be covered later. The BEMF per phase is described in equation 6 and 7 is generated by running a script to estimate the magnitude of BEMF for each phase (this script is included within APPENDIX-C).

Once the phase currents and BEMF values are known, it is possible to estimate the electrical power generated by the motor as described in equation 1. By dividing the mechanical speed of the motor it is possible to calculate the electrical torque produced at this point. The block diagram for this task is shown in Figure 18.

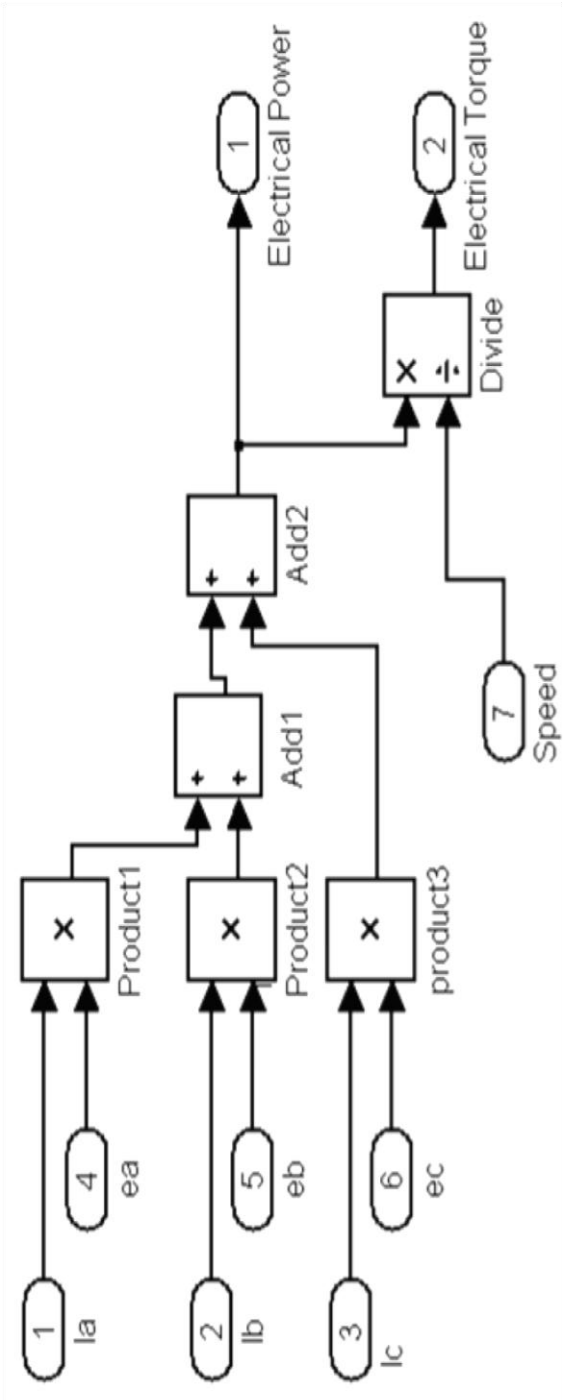

Figure 18 Torque estimator from current and BEMF signals

The whole electrical subsystem is depicted in Figure 19.

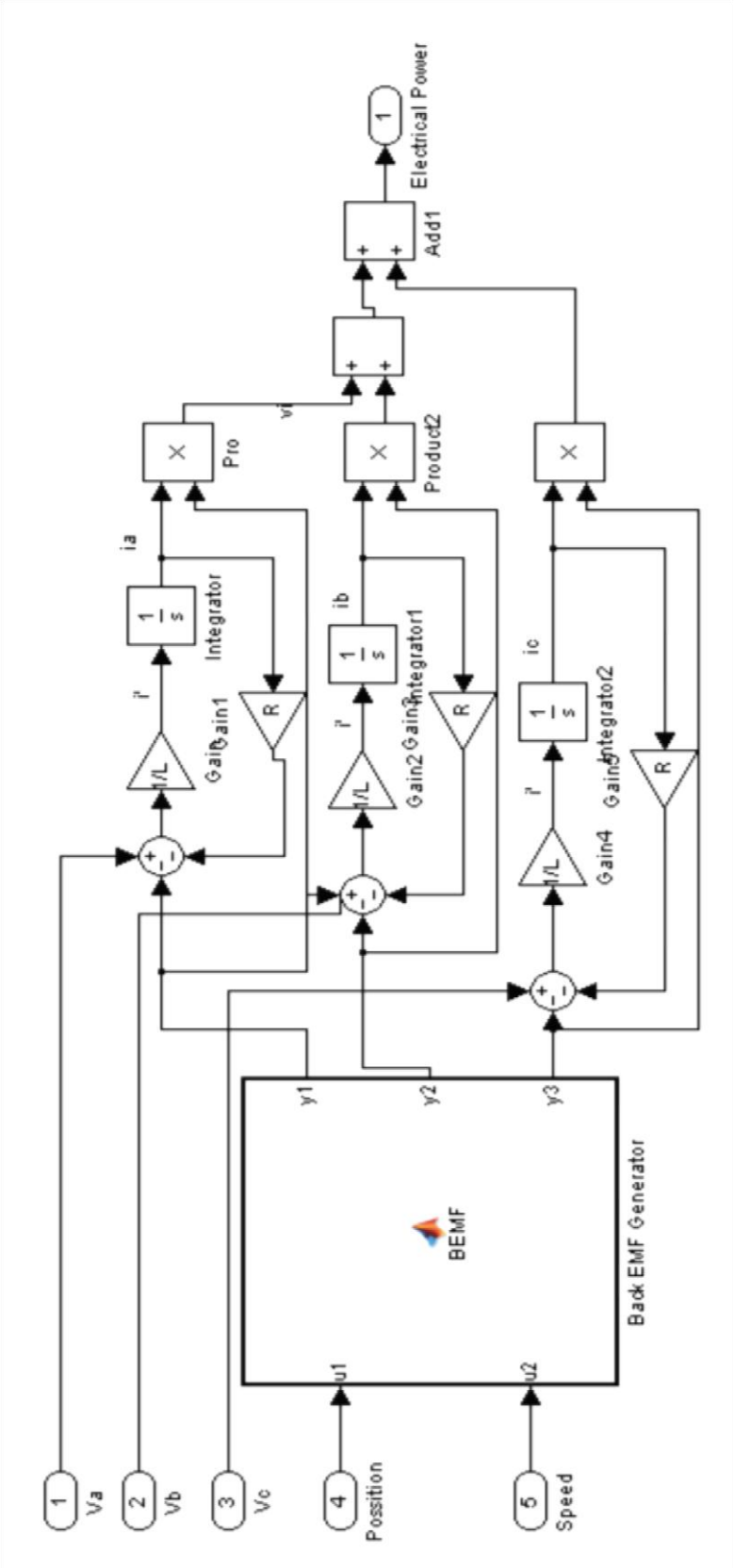

Figure 19 The complete model of the Electrical Subsystem

7.4 ESC [Electronic Speed Controller]

This subsystem is the brains behind the system as it contains the logic for commutation; feedback loops for speed control and calculates losses associated within the controller.

7.4.1 Hall Sensor Inputs

As mentioned earlier commutation is the process of manipulating the direction of current flow within the three phase motor in order to create a rotating field in the desired direction. The trapezoidal driving technique enables the controller to have the option to create one of six flux vectors depending upon the position of the rotor. The model is built with the assumption that three hall sensors are used to give six domains that the rotor occupies.

The mathematical model defining the system only outputs the mechanical speed of the rotor, but it is possible to model the hall sensor outputs by integrating the speed output of the mechanical portion of the simulator, once it has been converted to electrical speed from mechanical. This angle is then put through a recurring counter so that the position goes from 0 to 360 degrees. A second block then assigns this output a value between one and six depending upon its value for clockwise rotation as described by Table 8. This process can be seen in Figure 20.

Table 8 Hall sensor values

Rotor position θ_r	Output value	Equivalent Hall sensor output
$0^o<\theta_r<60^o$	1	100
$60^o<\theta_r<120^o$	2	101
$120^o<\theta_r<180^o$	3	001
$180^o<\theta_r<240^o$	4	011
$240^o<\theta_r<300^o$	5	010
$3000^o<\theta_r<360^o$	6	110

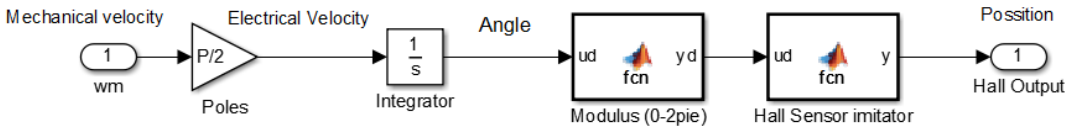

Figure 20 Hall Sensor Generation

7.4.2 Commutation Logic

The logic behind commutation is achieved by taking the reading from the Hall sensors[See Figure 21] and comparing it to a look up table[see Table 9] detailing which phases should be receiving power and of what polarity. Following usual convention the central node voltage potential is taken as half the supply voltage minus the sum of BEMF for each phase (21) from the controller because the central node is not grounded with the assumption that the phases are balanced [identical], meaning that each phase will receive half of the voltage seen at the input of the controller. Refer to table 8

Step Number	Effective Hall Sensor Output	Voltage to Phase a	Voltage to phase b	Voltage to Phase c
1	100	-Vin/2	Vin/2	Nc
2	101	Nc	Vin/2	-Vin/2
3	001	V/2	Nc	-Vin/2
4	011	Vin/2	- Vin/2	Nc
5	010	Nc	- Vin/2	Vin/2
6	110	-Vin/2	Nc	Vin/2

Table 9 Commutation look up table. Vin: total voltage to controller Nc: Not Connected

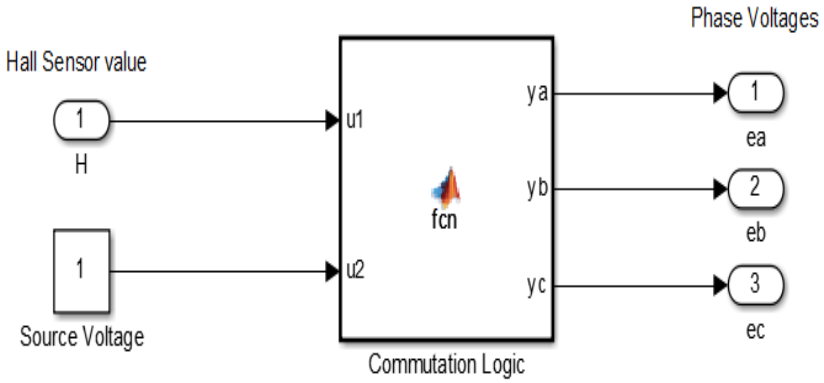

Figure 21 Commutation logic implemented basic

7.4.3 Power Control Feedback Loops

PID controllers have been commercially used since the early 1900's (22), and it is common for BLDC motors to have multiple feedback loops to control speed, torque or current. The most commonly implemented controllers are for the regulation of speed. It is not unusual for these feedback loops to neglect the derivative term resulting in a PI controller.

The first step for implementation of speed control is generating the error signal - with the simulation. It is possible to just pull a real time value for the actual speed from the mechanical portion of the simulator shown earlier in Figure 14 and compare it to the desired set speed. When this is coupled with a fine tuned PID controller for PAM or PWM power control, it will give excellent results for speed tracking. However it can be very misleading as when BLDC control is implemented in the reality, the speed can only be inferred from the hall sensors, which essentially gives an error signal which updates with each commutation step. This is simulated by taking note of the time taken for a commutation step by using a triggered sub system triggered by a commutation step. The subsystem outputs the time since the last trigger, then the mechanical speed is derived by multiplying by a factor that takes into account the number of poles and converts to mechanical rpm, as shown in Figure 22. The error signal is generated by calculating the error between desired set speed and actual speed.

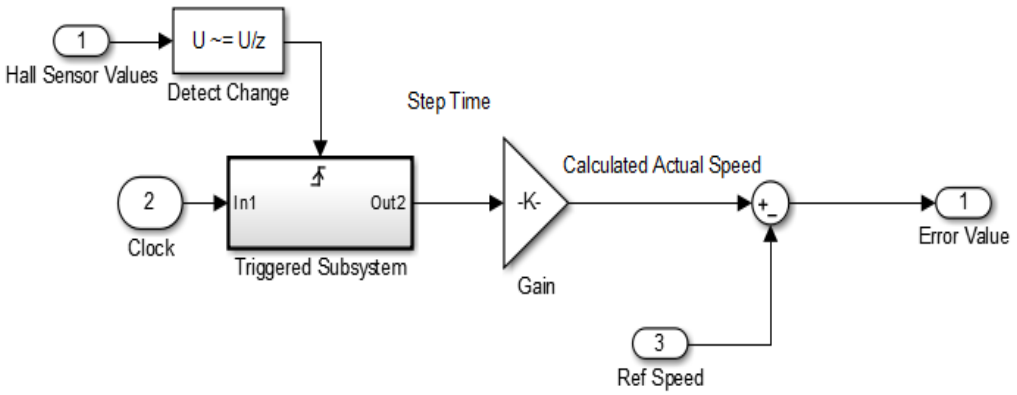

Figure 22 Generating error signal

The generation of the error signal is generic to all three power control techniques, but each technique will manipulate the voltage fed into the commutation block in its own way. The implementation of each technique is explained below.

The simulator contains everything necessary to simulate all three techniques, the technique of choice can be chosen by arming the appropriate block by setting the desired arming signal as described earlier in Table 2.

7.4.4 PAM Implementation

PAM changes the dc bus bar voltage to control power. The technique is modelled with the assumption that suitable smoothing circuitry is present to give ideal DC voltage after the bus bar controller. The error signal is fed into a PID block that outputs a value between zero and one, corresponding to the duty cycle of the power control semiconductor, with the assumption that the output voltage is directly proportional to the duty cycle. The bus bar voltage that feeds the commutation block is varied, as shown in Figure 23.

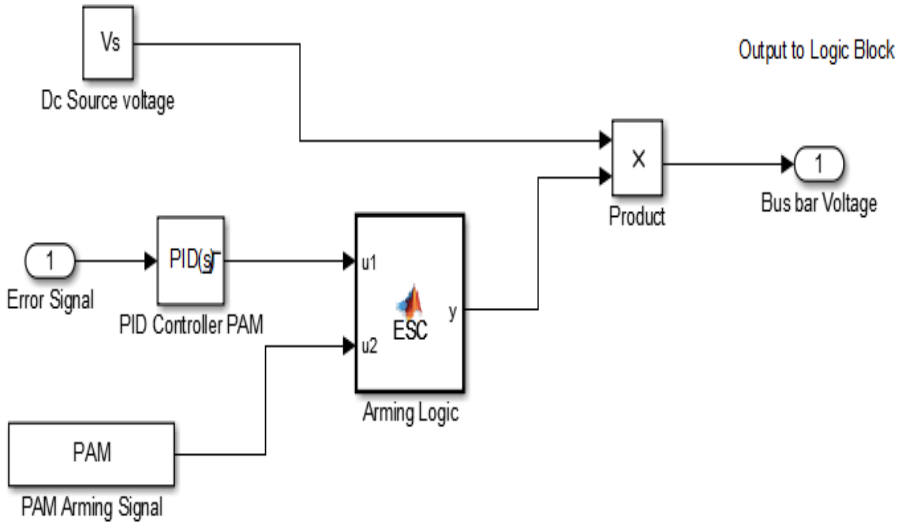

Figure 23 PAM bus bar control

7.4.5 PWM Implementation

With the assumption that the duty cycle is magnitudes higher than the commutation frequency and that hard chopping is selected [both high and low side devices undergo PWM]. The effect can be effectively simulated by applying the PWM externally to the input voltage fed into the controller. The controller then splits this between the correct phases, the output from the commutation block is the same as if the PWM was implemented internally.

The external representation of the PWM signal is generated by feeding the error signal into a PID block with output limits between zero and one. Comparing this value to a saw waveform of the same frequency of desired PWM with the maximum magnitude of one, the output from this has the same frequency and duty cycle of the desired PWM input. All that remains in the process is to multiply it by the input voltage that is accomplished within the same block that the arming signal is processed. The block diagram for this is shown in Figure 24.

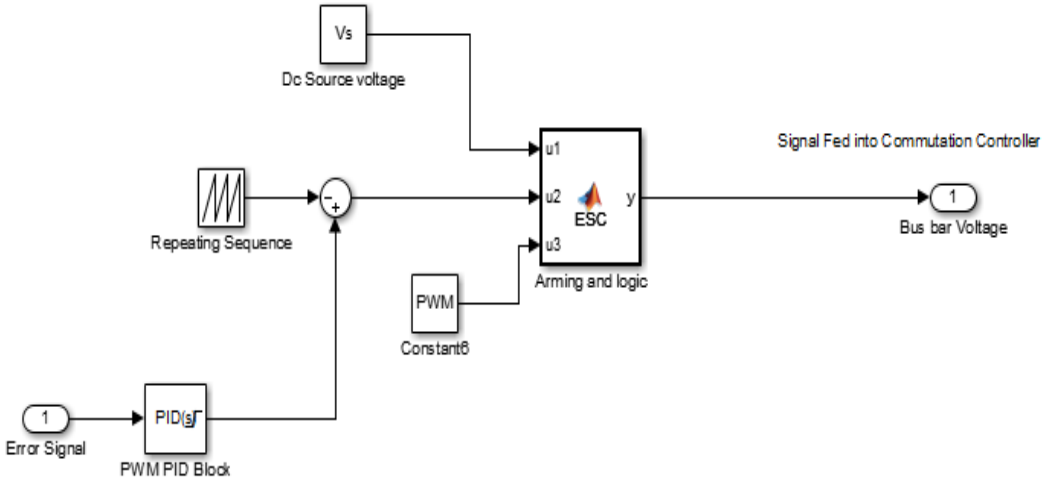

Figure 24 PWM implementation

7.4.6 CA Implementation

As previously detailed CA control works by controlling the angle of conduction [see Figure 25], with full power being the whole commutation step [60 degrees] and zero being angle of zero. However due to the cost impact of having a sensor capable of supplying such detailed angular information the technique is instead implemented within the time domain. The controller estimated the time for the commutation step by using a sub system triggered by a commutation step, the subsystem outputs the time since the last trigger giving a good estimate for the previous commutation step time. The CA controller then calculates the dead time dependent upon the feedback signal.

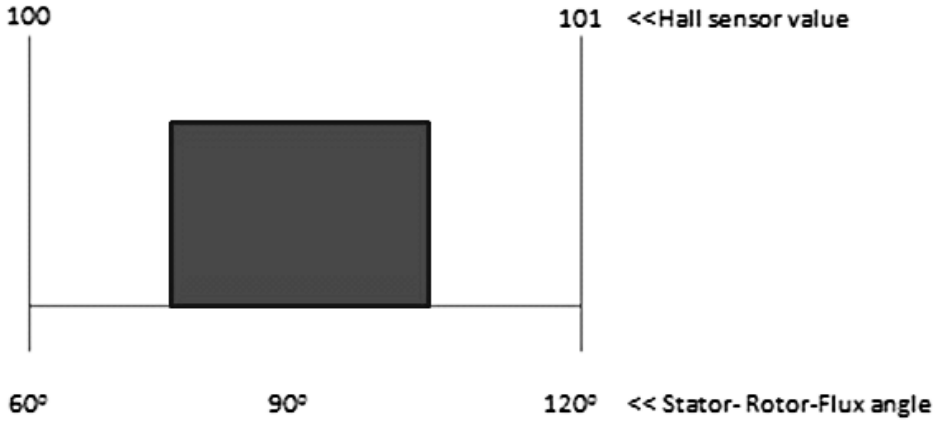

Figure 25 Conduction angle (theoretical)

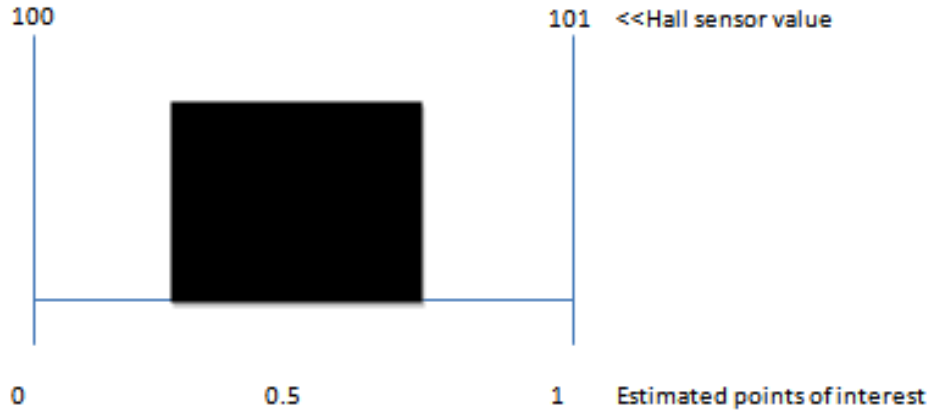

Figure 26 CA applied in time domain, 0 ,5,1 represent estimated commutation mid point and end point

To iterate the CA is implemented in such a way that it outputs a signal that is connected to the commutation block. The commutation block only applies a voltage to a phase if it both satisfies the commutation logic and, the CA blocks output confirms that the signal is within the conduction time. Otherwise the phase will not receive power from the H-bridge. The block diagram for this process can be seen in Figure 27.

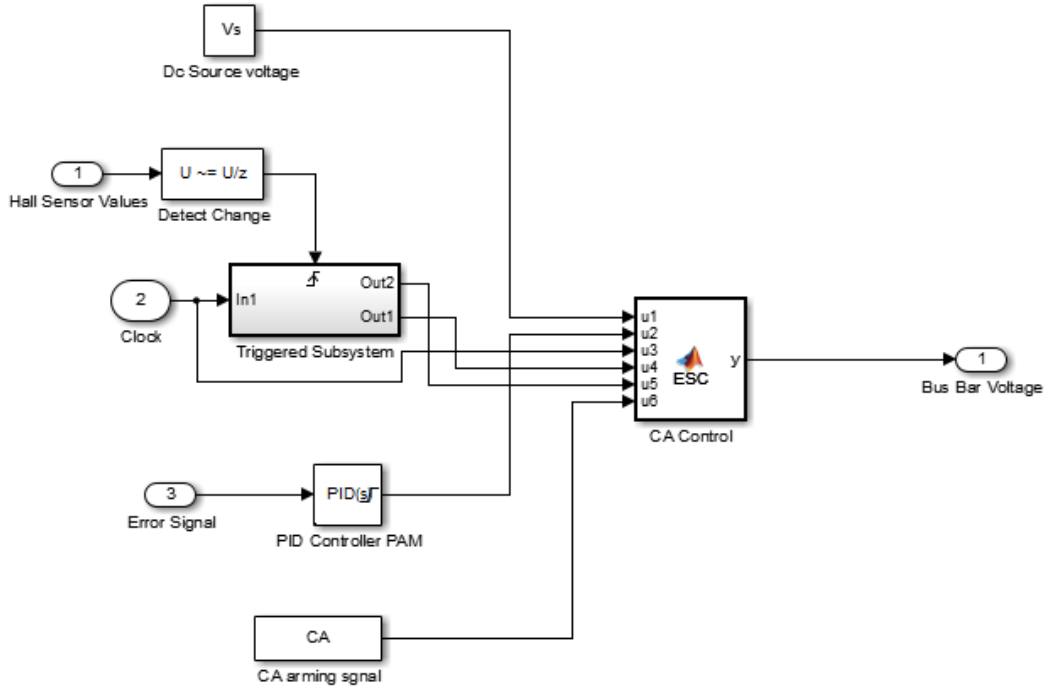

Figure 27 CA implementation

7.4.7 Controller Losses

As mentioned earlier many simulators model the speed controller as an ideal device. However in reality it is not, for some applications modelling it in this manor will still yield accurate results in some systems. However in the case of a systems with a low voltage source (dc battery for example). The voltage drop associated with the controller can amount to a significant percent of the available driving voltage (21), in scenarios such as this it is not sensible to model the ESC as ideal.

With respect to the simulator this means that the motor windings do not see the full source voltage but instead have a lesser potential due to the voltage drop across the controller. There are many losses associated with ESC's, with the most common being related to the digital circuit controlling the logic. However because this is generic to every controller these power consumptions can be ignored, shifting the area of interest to the losses associated with the high power side of the controller. The controller is the part that deals with the high currents and voltages, this side is comprised of a three phase H-Bridge, using semiconductors as the active switches.

The losses associated with the H-bridge arise from both power control and commutation. The MOSFETs themselves are not ideal devices and have losses, the three main losses can be summarised as follows:

- Conduction losses
- Switching losses
- Gate charge loss

It is common for the gate charge losses to be neglected as they pale in comparison to conduction and switching losses. This simulator will neglect the gate charge losses.

7.4.7.1 Conduction Losses

Conduction losses are the losses associated with the period of conduction, commonly referred to as resistive or copper losses - as they are just that. The losses are related to the resistance of the semiconductor and can be calculated in just the same way. The voltage drop is described by equation 8 and the power dissipation by equation 9 (23). The values for a semiconductor resistance can be found within its data sheet; however the common value can be misleading as it gives the value for a cool device. The resistance is a function of temperature and should be calculated from the data sheet for a reasonable operating temperature.

$$V=IR \quad [8]$$

$$P= I^2R \quad [9]$$

With the assumption that both the high side and low side semiconductors that populate the H-bridge are identical, the phases remain balanced and the central node voltage assumption still stands. If the simulator was to run at a duty cycle of unity, the extra resistance from the H-bridge could simply be added to the resistance of the phases and the electrical portion of the simulator would then take these losses into account. However, unlike the resistive portion of the phases that is present at all times, the resistive losses of the H-bridge only arise during conduction.

This problem is overcome by calculating and applying the voltage drop from the H-bridge by inserting a block following the commutation block before the electrical portion of the simulator that converts the voltage input into equivalent currents as shown in Figure 28.

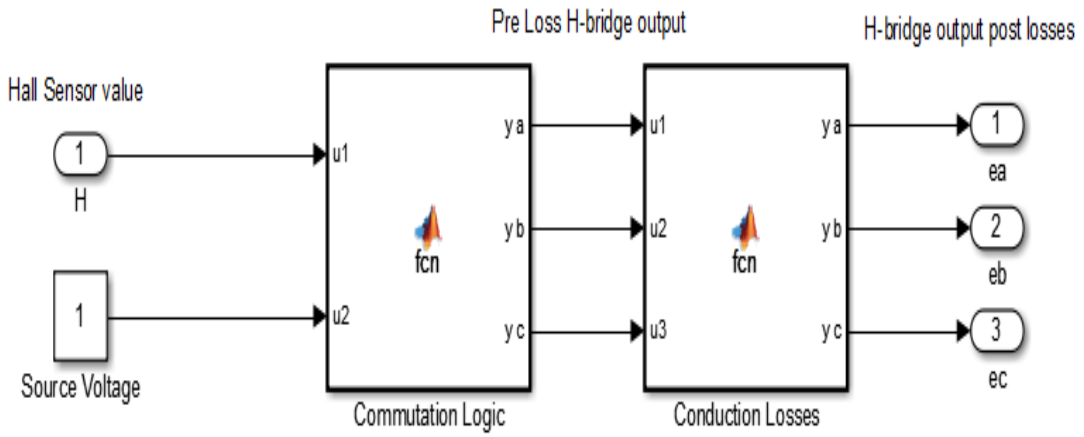

Figure 28 Conduction losses

The voltage drop is calculated for each phase by multiplying the resistive value of the semiconductor by the current flow in the particular phase it is powering during its conduction period. This voltage drop is then subtracted from the relevant H-bridge output voltage - the block diagram powering this activity can be seen in Figure 29. The block responsible of calculating voltage losses also outputs an instantaneous value for total conduction power loss.

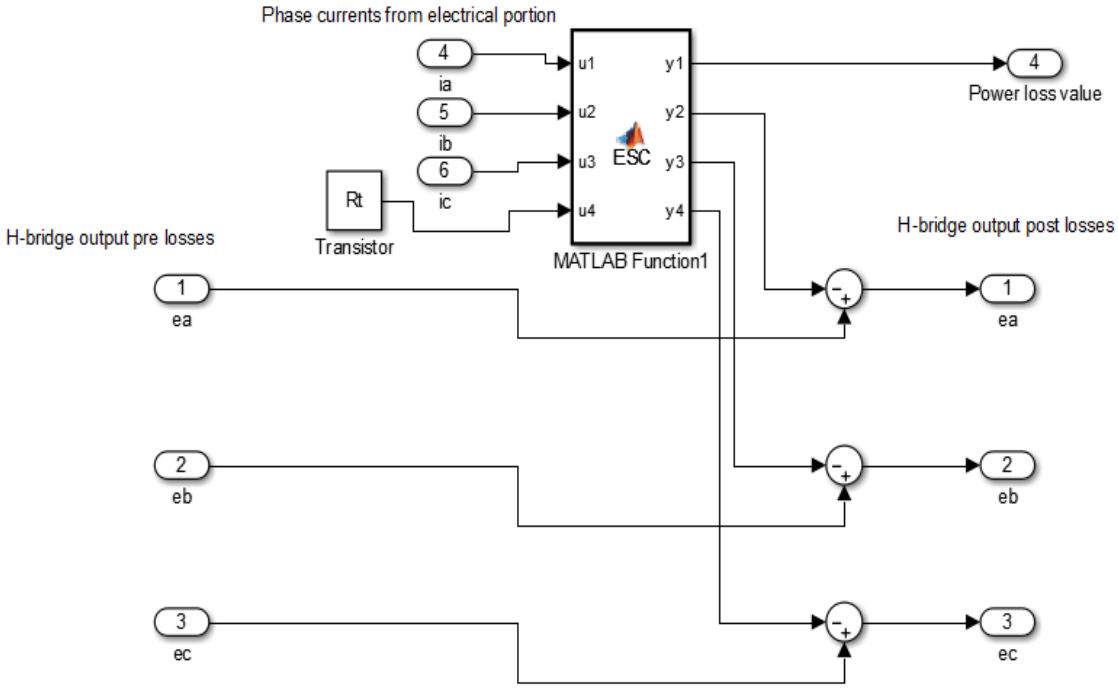

Figure 29 H-bridge conduction losses implementation

Due to the PAM power control technique including an additional semiconductor to control power, it is obvious that the above model does not take this into account. So built into the PAM power control block is another loss block to take this into account, implemented in a similar manner it can be seen in Figure 30.

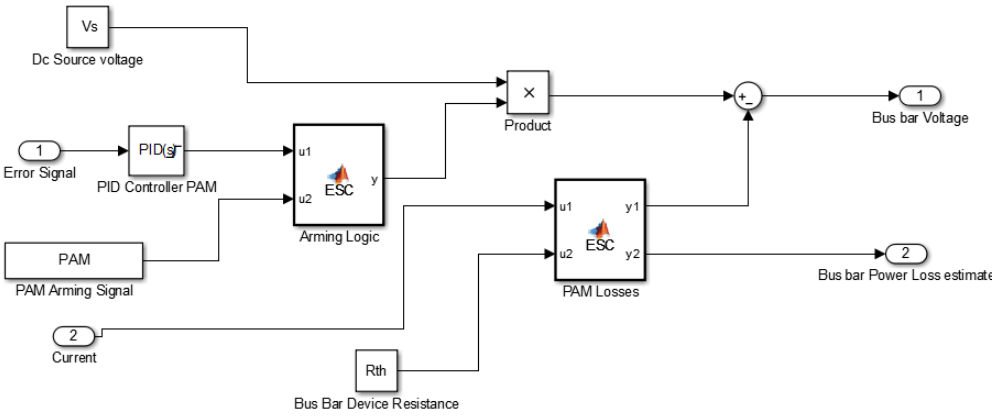

Figure 30 Extra conduction losses arising from PAM

7.4.4.2 Switching Losses

The losses arising from switching are largely dependent upon the current flowing through the device and the switching frequency. It is possible to estimate the power loss arising from switching [Pswitch] by using equation [10]. The values for rise and fall time [Trise,Tfall] are contained within the semiconductors data sheet and fswi is the driving frequency.

$$Pswitch = 0.5 \times VDS \times ID \times (trise + tfall) \times fswi \quad [10]$$

VDS represents the voltage potential between the drain and source of the semiconductor; this can be approximated for the H-bridge as half of the source voltage minus the BEMF arising from the relevant side of the motor windings. Because two semiconductors conduction at any one time [high side and low side], the equation for losses can be simplified to give the total loss for the H-brigde as a function of buss bar voltage and BEMF. The frequency of switching will vary for each technique: with PWM the frequency will be the PWM frequency; with CA it will be the commutation frequency as shown in equation [11]. The value for ID is calculated as an average over more than one commutation step.

Again because PAM includes an additional semiconductor, the losses associated with it must be included. The technique will suffer the losses from the switching associated with commutation as in equation[10], along with the losses for the additional semiconductor. This has its own switching frequency and different fall and rise times that are defined in the command window pre simulation. The VDS for this switch will be the source voltage minus the buss bar voltage, leading to the PAM switching losses being defined by equation [12].

H-Pswitch-PWM = 0.5 × ID × (H-tonoff) × H-Freq x(Vbus-BEMF) [10]

H-Pswitch-CA=0.5 × ID × (H -tonoff) × Comutation freq x(Vbus-BEMF) [11]

PAM Switching Losses = H-Pswitch-CA + (0.5 × ID × (trise + tfall) × fswPAM x(Vs-Vbus)) [12]

This has been implemented as block diagram, depending upon the arming signal, the switching losses block calculates the appropriate losses.

8 Simulator Testing

In order for the simulation results to be of any use, the Simulator must first be proved working and accurate. This section details the process of how this was achieved, starting by performing preliminary tests to check the basic operation of simulations is as expected, and later goes on to compare to results from other literature sources.

The following simulations are run on MATALB Simulink version R2012b, using default Solver od45 with tolerance of 1e-6.

8.1 Preliminary Tests

For this section of tests the Maxon EC 6 215550 BLDC motor is simulated not taking into account controller losses, using the values shown in Table 10. The preliminary tests alter one of the parameters at a time keeping the rest constant to observe if the system reacts as expected.

Motor Data Maxon EC 6 215550	units	value
Number of poles	n/a	2
Assigned Power rating	Watts	1.2
Nominal Voltage	Volts	6
No Load Speed	Rpm	47130
Stall Torque	mNm	0.5
No Load Current	mA	60
Phase Resistance	Ohm	6.25
Phase Inductance	mH	0.0455
Rotor Inertia	Kg.m2	5e-10
Friction Constant	Nm.s	1.38e-8
BEMF constant	Vs/Rad	1.05e-3

Table 10- Example Motor 1 Data ,Maxon EC 6 215550 BLDC

As a standard for comparison the simulator is ran with the values shown in Table 10. Figure 31 shows the speed vs time for the system when running at full power from standstill. It can be seen the system accelerates and reaches steady state when the losses from friction equal the electrical torque generated by the motor as expected.

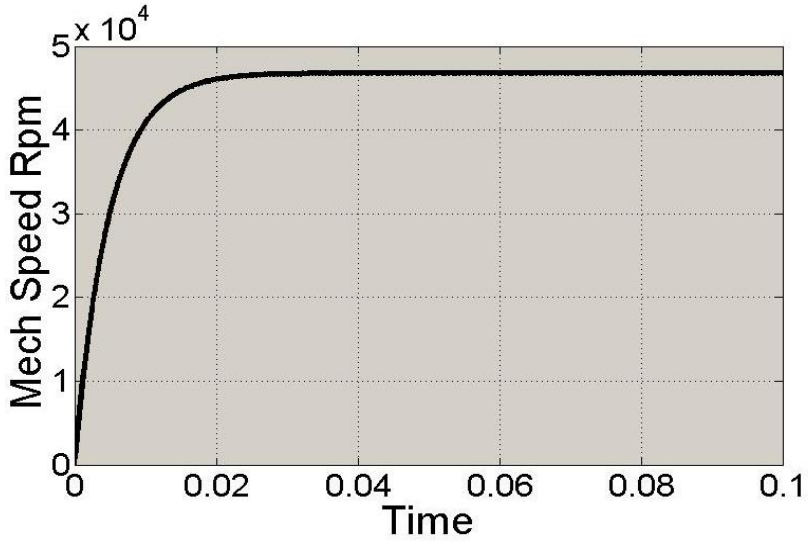

Figure 31 - System reaction to full power, time speed

8.1.1 Voltage Source

For the purpose of this test all variables remain the same except the source voltage which is doubled, if the system is operating as expected the Steady State (S.S) speed should increase as can be seen in Figure 32.

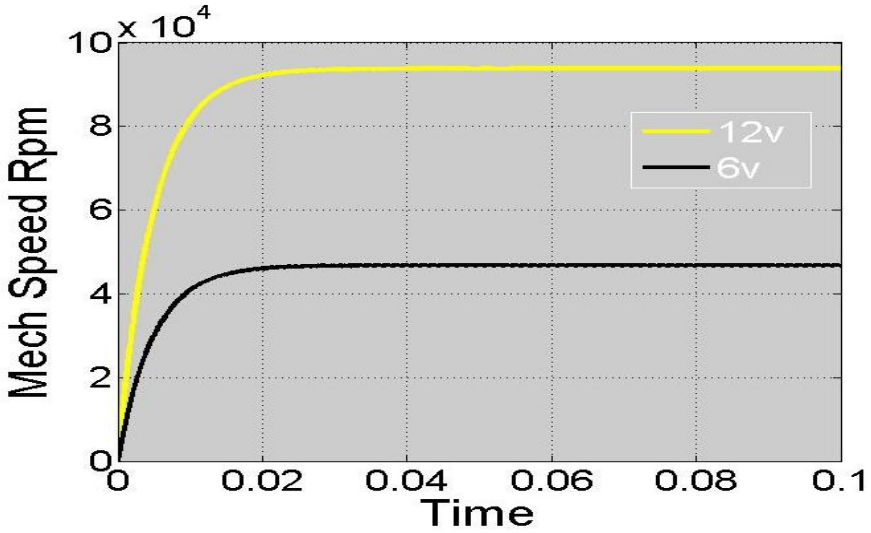

Figure 32 Voltage effect on s.s

8.12 Frictional Constant

For the purpose of this simulation the friction constant is increased by a factor of 100 and the reaction of the system observed, as expected the S.S speed decreases [see Figure 33]

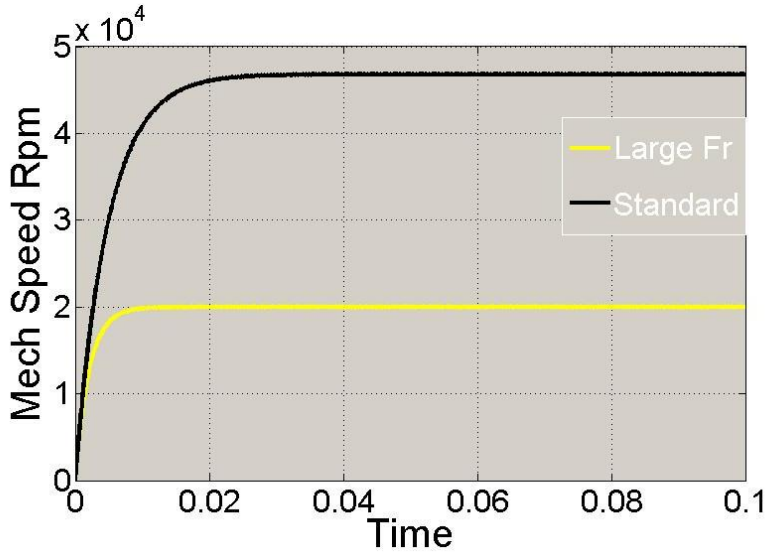

Figure 33 Effects of friction

8.1.3 Rotor Inertia

The inertia of a system should not affect the S.S speed of said system, just the time it takes to reach S.S, Figure 34 shows the response of the system if the inertia value is doubled from its original value.

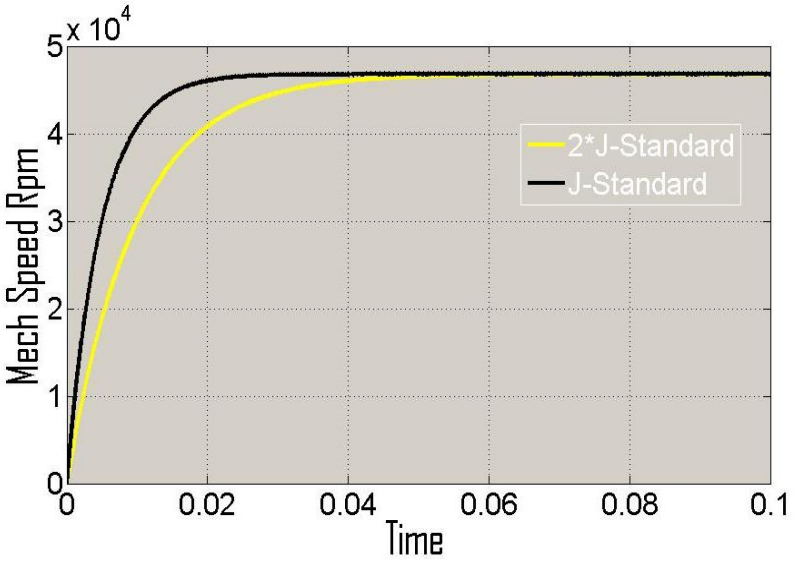

Figure 34 Effects of inertia

As expected the system reaches the same S.S speed but the time constant has increased.

8.14 Reaction to Load

In this simulation a load of 0.25 mNm [half of its stall torque]is applied to the system at 0.1 seconds, in this period the speed should decay to another new S.S value, Figure 35 shows the results of the simulation behaving as expected.

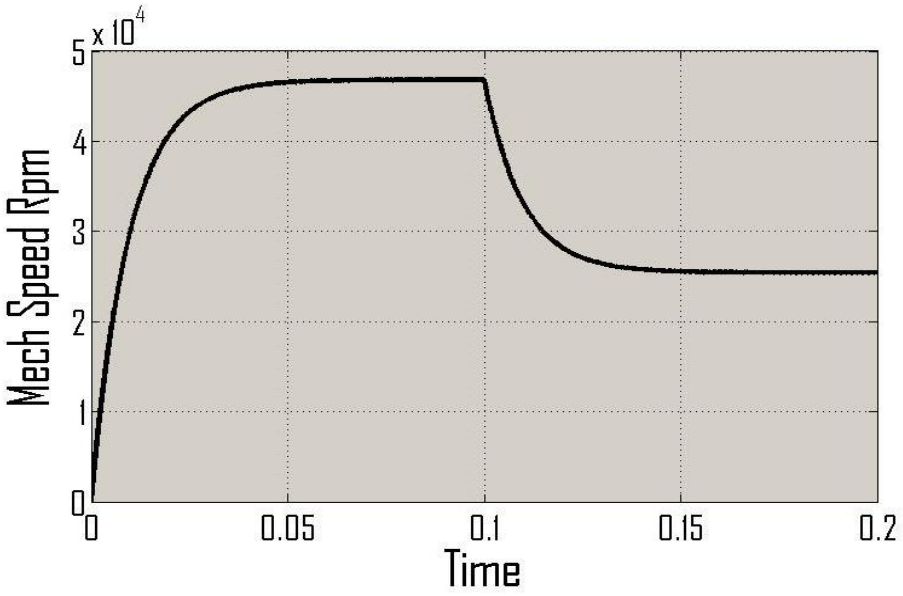

Figure 35 Reaction to reasonable Load

Another Area of interest is the current within the motor, Figure 36 Shows the average current within the motor for the above test, notice how the current is initially high when the system is accelerating, decreases once S.S is reached and again climbs in order to power the load as expected

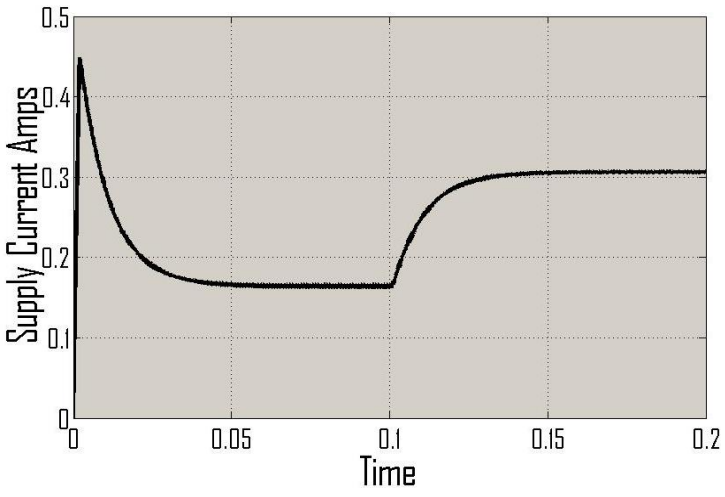

Figure 36 Dc source current

8.2 Control Strategies [Open Loop]

The previous tests have been run at full power [open loop no feedback] using the traditional PAM model. Two other techniques have been modelled traditional hard switching PWM and CA (conduction angle), however theoretically all three techniques behave the same at a duty cycle of unity.

Figure 37, Figure 38 and Figure 39 show the open loop reaction to an open loop input of 100% of all three techniques [not taking into account controller losses at this stage]. As expected the systems all react similarly having identical time constants and S.S values.

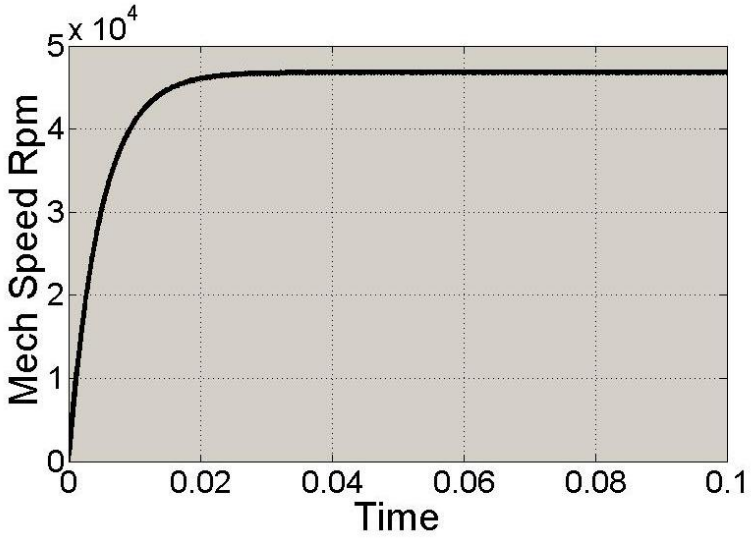

Figure 37 PWM Open loop response to full input

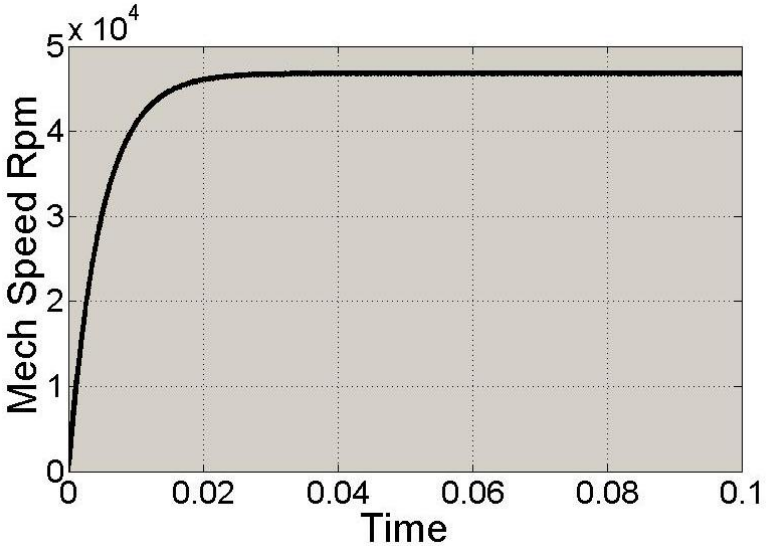

Figure 38 PAM Open loop response to full input

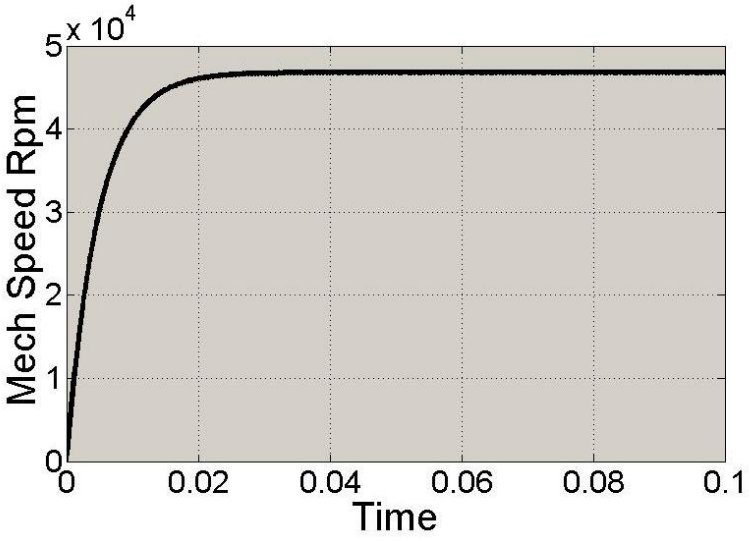

Figure 39 CA Open loop response to full input

The input of the system was then set to 80% in open loop mode, by referring to the figures, Figure 40, Figure 41 and Figure 42 that show this response it can be seen that again all three techniques have the same S.S speed and time constants.

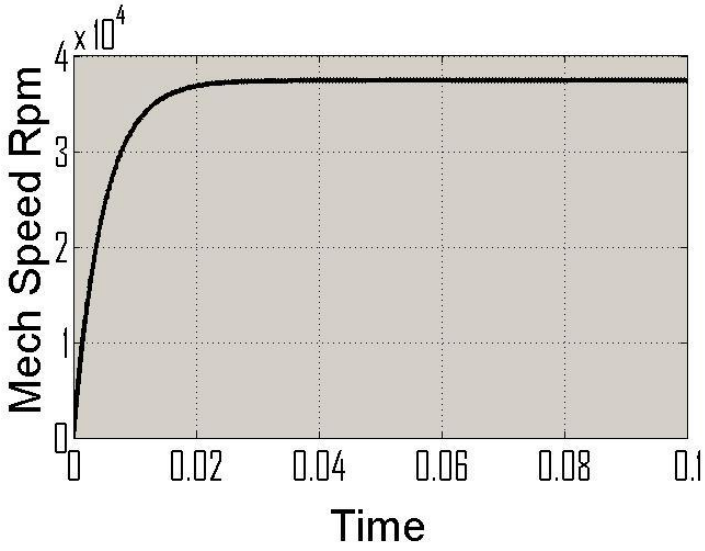

Figure 40 Open Loop PAM Control 80%

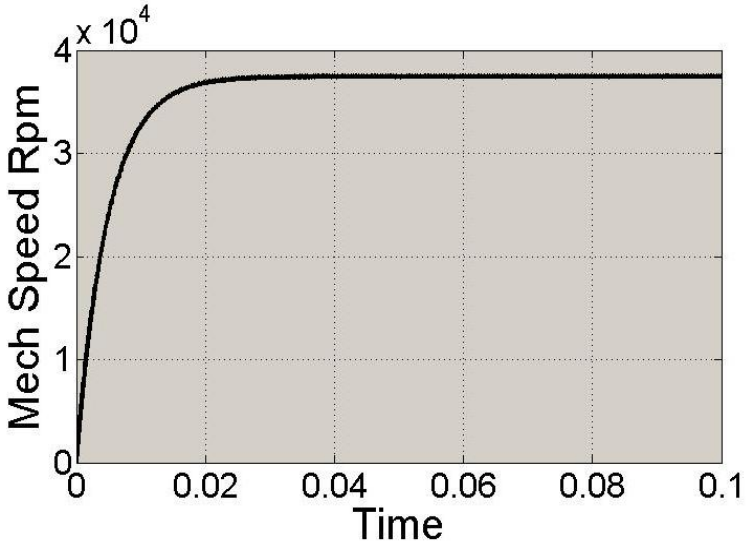

Figure 41 Open loop PWM control 80%

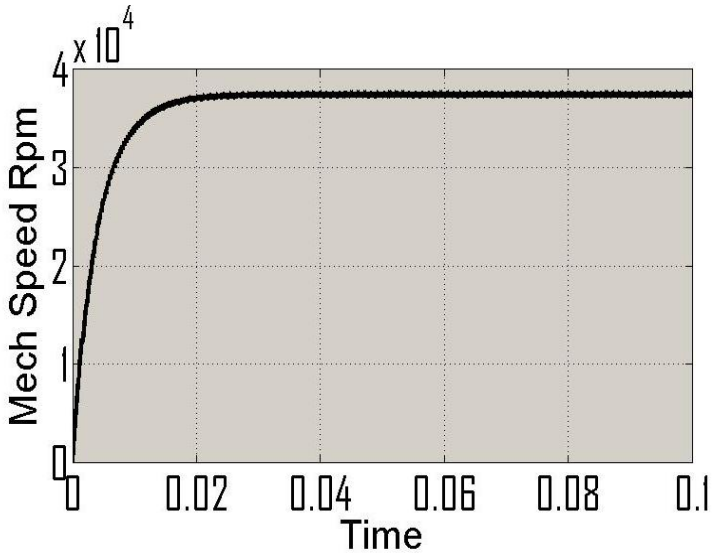

Figure 42 Open loop Ca control 80%

Figure 43, Figure 44 and Figure 45 are zoomed in views of the speed when running at 80% open loop for all three techniques, the figures depicting PAM and PWM show the effect of torque ripple form commutation, then by comparing these against the figure for CA it is possible to see the additional torque ripple caused by this technique, but the average speed remains the same for all techniques.

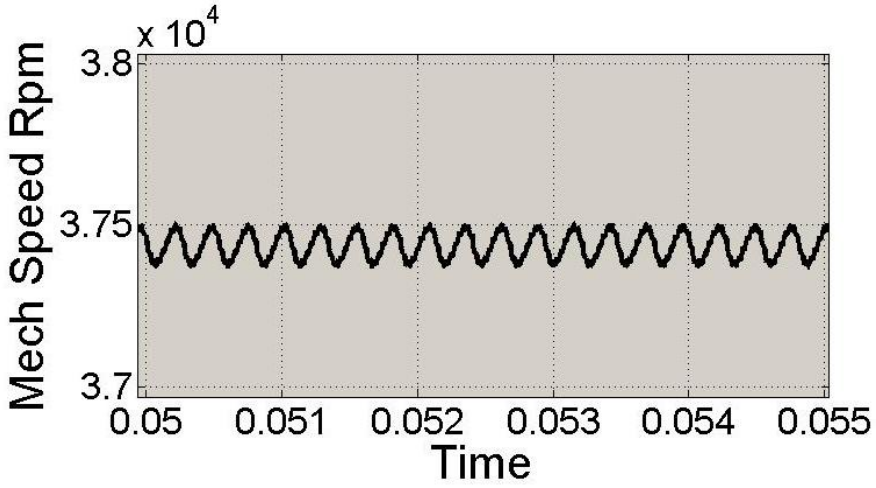

Figure 43 PAM Zoomed

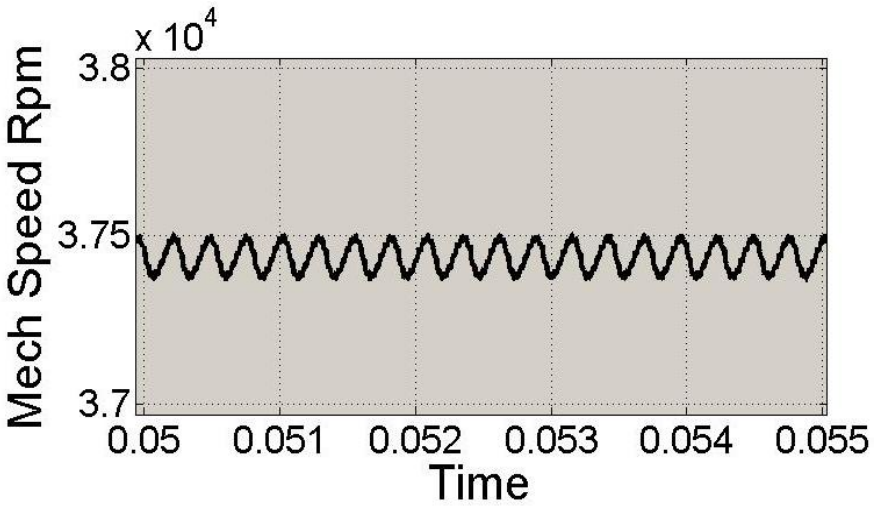

Figure 44 PWM zoomed

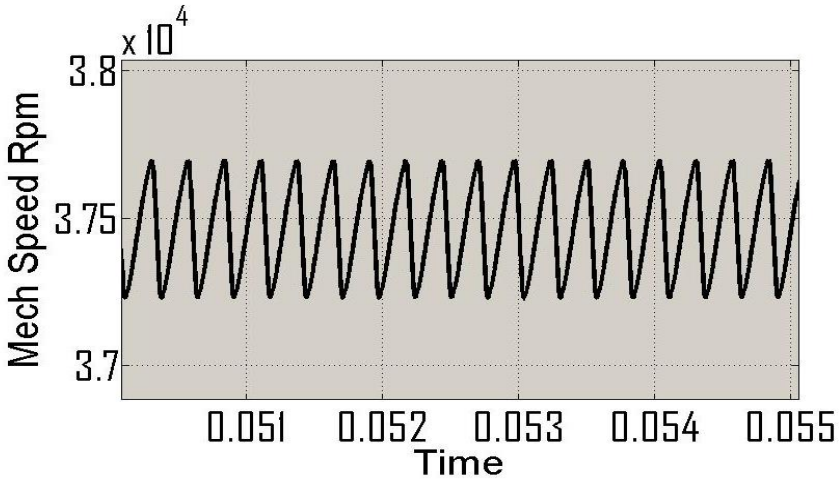

Figure 45 CA zoomed

If the open loop input is reduced yet again it would be expected that the S.S speed would decrease. Speed ripple from commutation should stay relatively small and the speed ripple for CA control should increase.

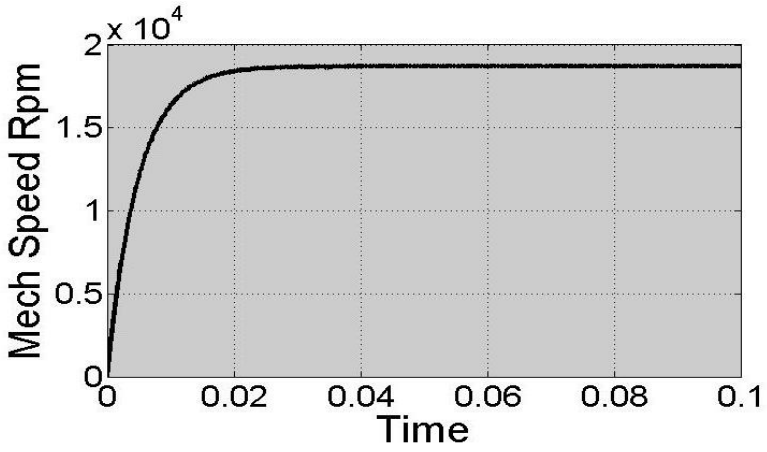

Figure 46 and Figure 47 show the open loop response of the system to a closed loop input of 40% for PAM and CA control respectively. It can be seen that they both reach the same S.S, and the speed variations for CA are becoming apparent even from a distance. Figure 48 and Figure 49 are close ups for the same 40% simulation. It can be seen that the ripple for PAM control is similar to that of the 80% simulation [see Figure 43] as expected, and that CA control exhibits speed fluctuations that are greater than those caused just by commutation and decrease with duty cycle as expected.

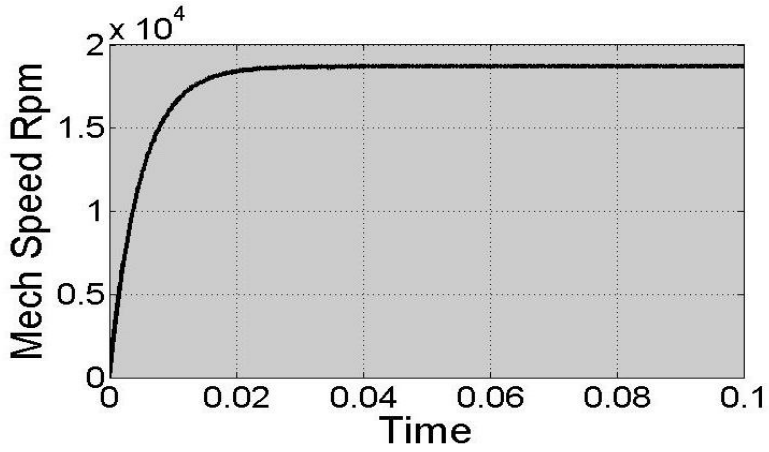

Figure 46 Open loop PAM control 40%

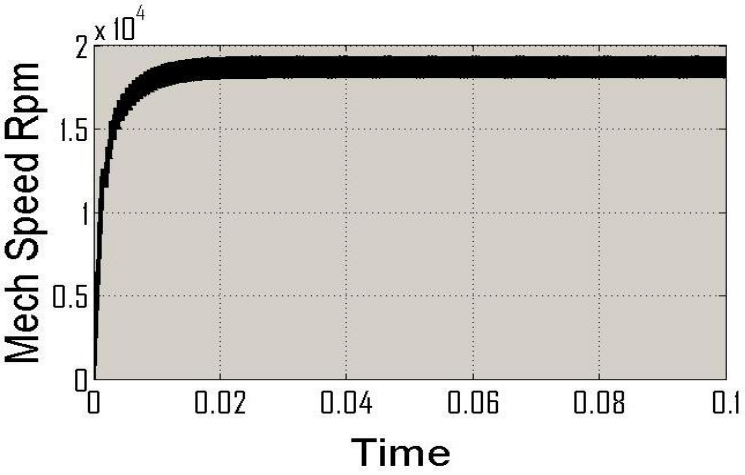

Figure 47 Open loop CA control 40%

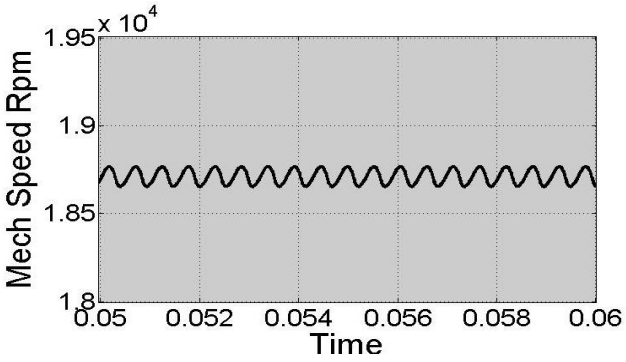

Figure 48 PAM 40% zoomed

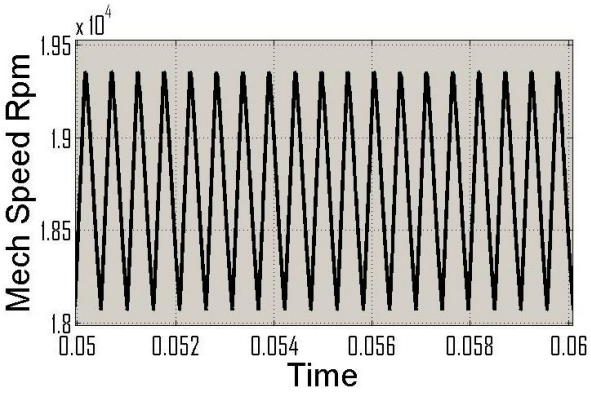

Figure 49 CA open loop 40% zoomed

8.3 Control Strategies [Closed Loop]

The simulator has PI control loops built in (as discussed in chapter-7) to control speed. As at this stage their basic operation is only being proved the constants for the controller are found by trial and error. These values can be seen in Table 11. Figure 50,

Figure 51 and Figure 52 show each of the control techniques attempt to maintain a speed of 25,000 rpm under no load condition, roughly equalling around 60% maximum speed. As it can be seen each technique tracks the desired speed closely proving the basic operation of the control loops.

Table 11 Control loop gains

Control Strategy	Kp	Ki
PAM	2.2e-5	5e-3
PWM	2.2e-5	5e-3
CA	2.2e-5	5e-3

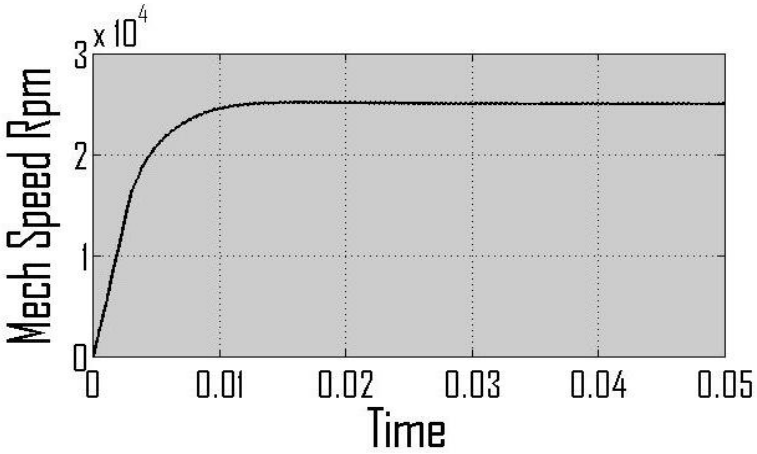

Figure 50 PAM feedback loop set speed of 2.5e4 Rpm

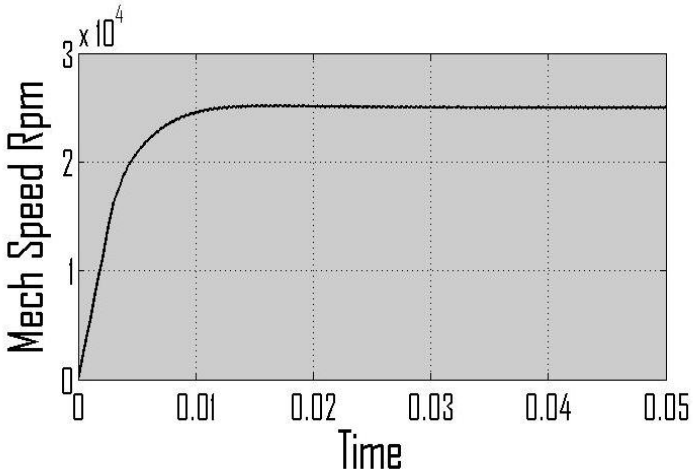

Figure 51 PWM feedback loop set speed of 2.5e4 Rpm

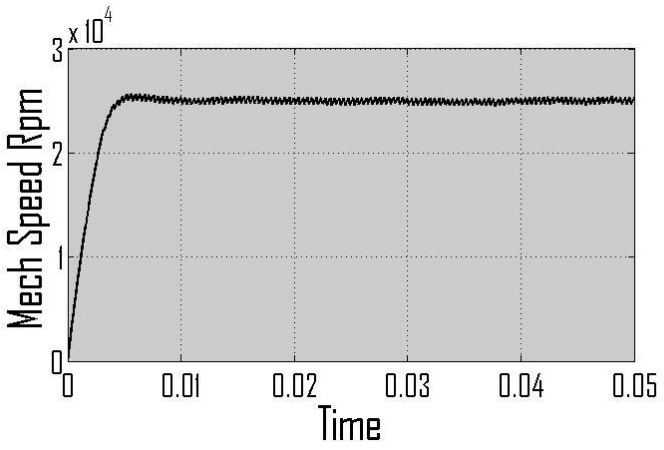

Figure 52 CA feedback loop set speed of 2.5e4 Rpm

8.4 Controller Losses

This section tests that the losses from the controller act as expected. It is expected that taking into account the conduction losses within the controller would result in a lower top speed as it reduces the effective voltage seen by the motor. The effect of on state resistance on PWM and CA control strategies ran in full power open loop operation is shown in Figure 53. The expected relationship is true where PAM requires an extra semiconductor as discussed. This also has conduction losses that are additional to the conduction losses from the H-bridge. Figure 53 shows the effect of varying the ESC's on state resistance on speed, as expected, it decreases the top speed.

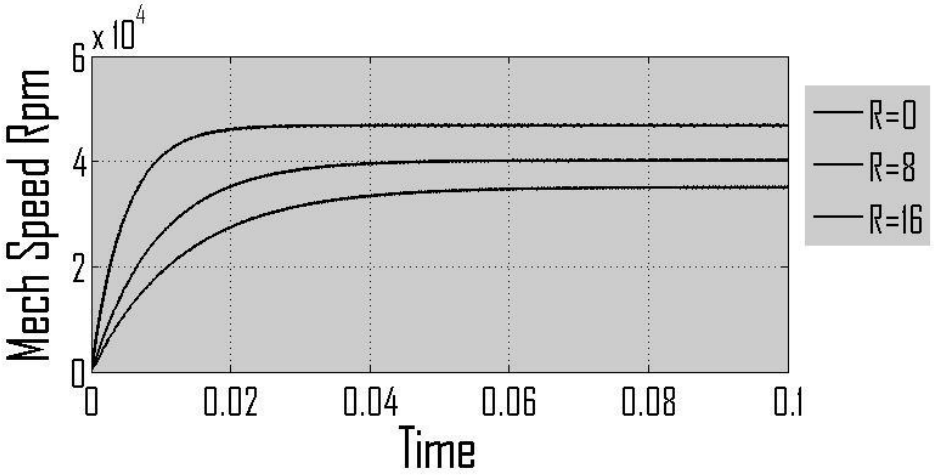

Figure 53 Effect of H Bridge resistance

8.5 Simulator Accuracy

The test shown in the previous section only show the general behaviour of the system is as expected. However it is still necessary to show the Simulator accurately simulates the system.

By comparing to literature on other simulators such as in Reference- (5), it is possible to evaluate the accuracy of Simulations. Reference- (5) used the maxon EC 6 motor as a test subject, and compares the results of simulations to key data given in the data sheet, main data is shown in Table 12 gained from data sheet included in APPENDIX-A.

Table 12 Motor values

Motor Data Maxon EC 6 215550	units	value
Number of poles	n/a	2
Assigned Power rating	Watts	1.2
Nominal Voltage	Volts	6
No Load Speed	Rpm	47130
Stall Torque	mNm	0.5
No Load Current	mA	60
Phase Resistance	Ohm	6.25
Phase Inductance	mH	0.0455
Rotor Inertia	Kg.m2	5e-10
Friction Constant	Nm.s	1.38e-8
BEMF constant	Vs/Rad	1.05e-3

In Reference- (5) the system is ran at full power from standstill until S.S has been reached, then at a time of 0.05 seconds a torque load is introduced as a unit step of 0.23 mNm, and left until a new S.S has been reached. The plots of time vs speed, time vs electrical torque and time vs bus bar current are taken and presented in the literature, Figure 54,Figure 55 and Figure 56 are images of these results.

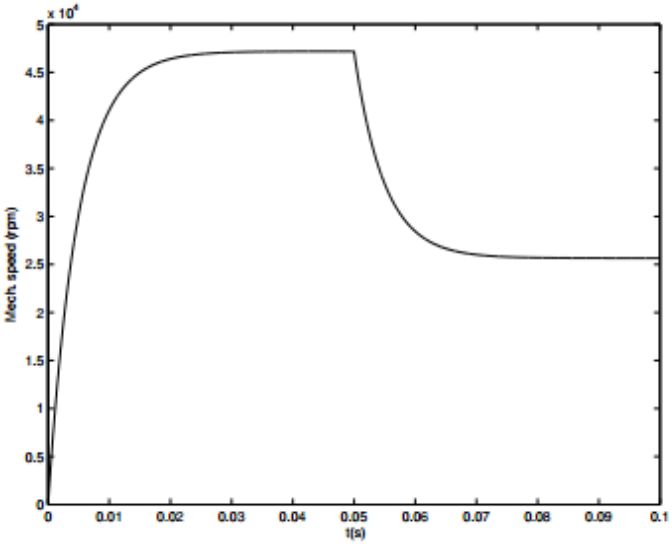

Figure 54 Motor speed literature

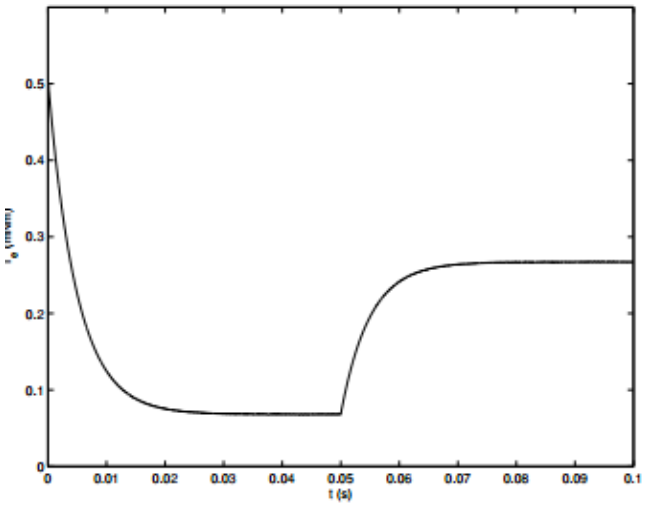

Figure 55 Electrical torque literature

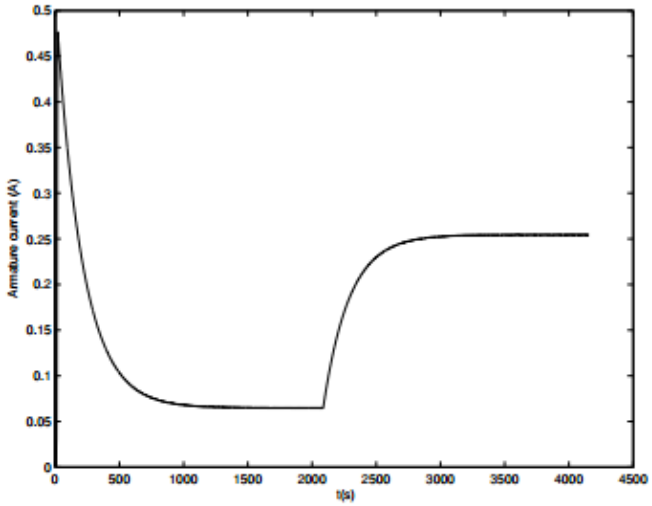

Figure 56 Source current literature

The same test as above was performed using the simulator outlined in previous chapters and the results shown in Figure 57, Figure 59 and Figure 58. By comparing results it can be seen that the simulator is acting as expected with no visible contradictions to proven results.

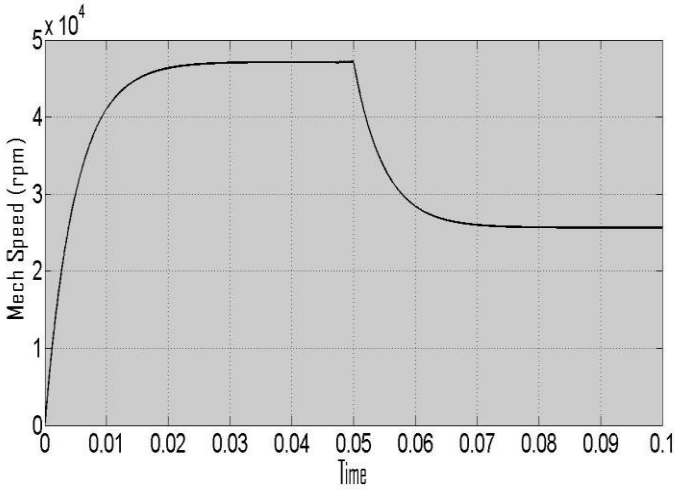

Figure 57 Speed reaction simulation

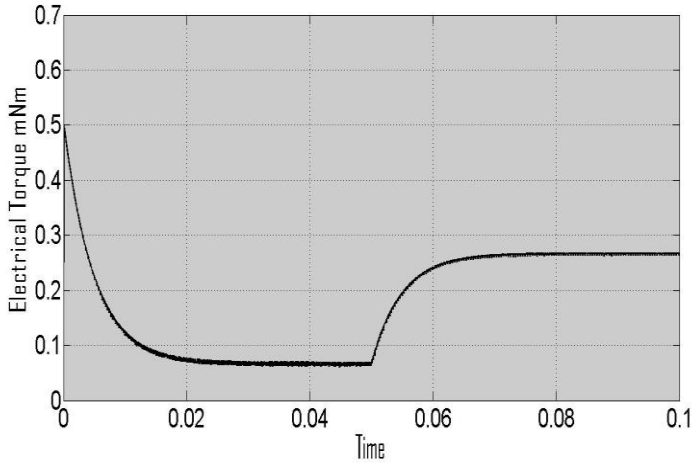

Figure 58 Electrical torque simulation

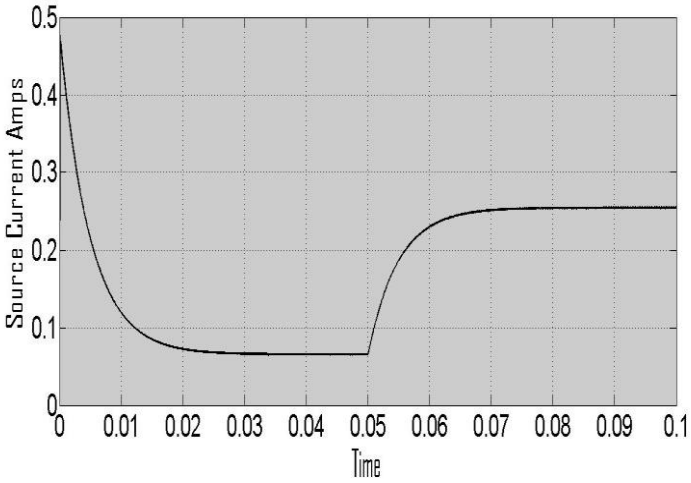

Figure 59 Source current simulation

Chapter 9: Simulation Results

This chapter introduces the test carried out by simulation, expands on why each area of interest is important in assessing the novel technique. Because the motor is often connected to a real system with an associated inertia the following simulations are ran with an inflated combined inertia of a magnitude larger than that of just the motor alone.

The proposed technique is measured and compared against the more common PWM style; PAM has been omitted from the comparison due to its requirements for additional components and related costs of manufacture. The input variables required to operate the simulator inputted through the command window are included within APPENDIX-D for each main simulation, any other relevant changes implemented at block diagram lever are explained in each sub chapter.

9.1 Speed variation

Commonly a smooth power delivery is desired however in the real world speed fluctuations find their way into BLDC drive systems in the form of torque ripple mainly from commutation steps, the proposed technique also introduces additional ripples from its macro power control style. The simulations carried out in this section are aimed at expressing this graphically.

Two sets of simulations are carried out on both PWM and CA in order for comparison. Firstly the motor is simulated under no load condition at a reference duty cycle of one, this duty cycle is then reduced to zero using inversed ramp function and the motor speed over time tracked as shown in Figure 60 and Figure 61. This allows the speed fluctuation as a function of duty cycle to be calculated and displayed graphically [Figure 62, Figure 63]. Running a relatively long simulation time of one second and ramping the duty cycle down slowly from unity to zero over the simulation period gives a large number of commutation steps per duty cycle value, this makes it possible to accurately relate the time to duty cycle within the broad range of the simulation.

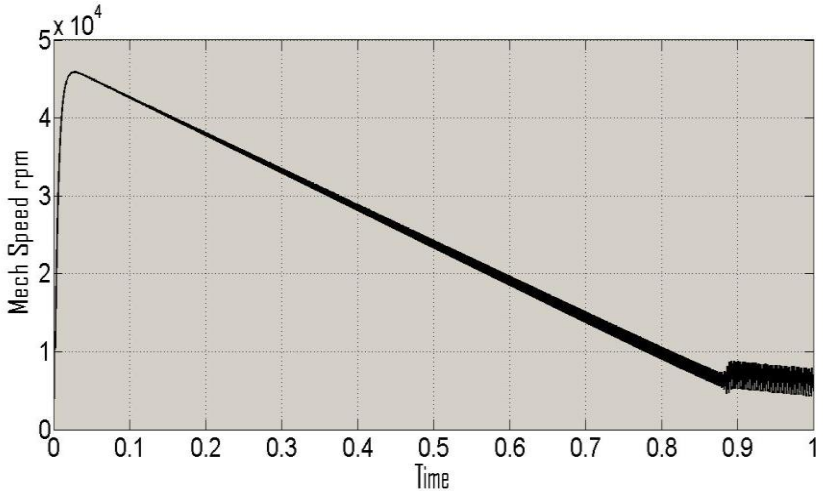

Figure 60 Speed response for decrease in duty cycle for CA

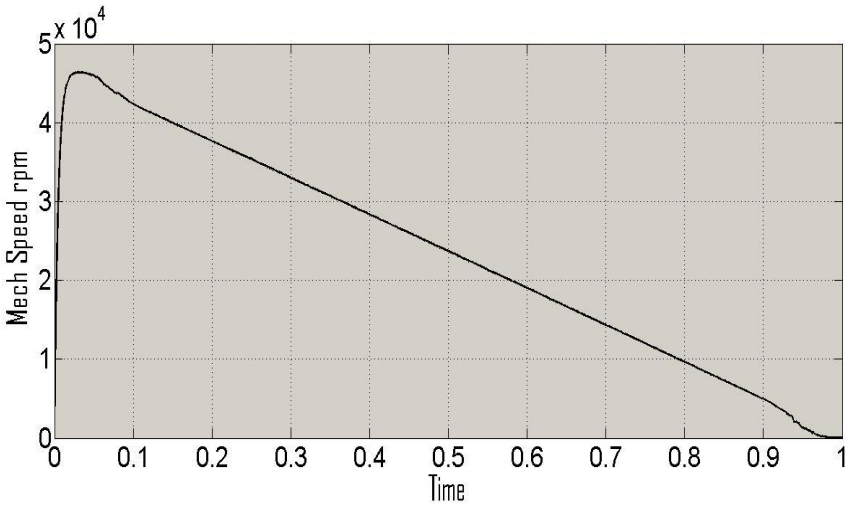

Figure 61 Speed response for decrease in duty cycle for PWM

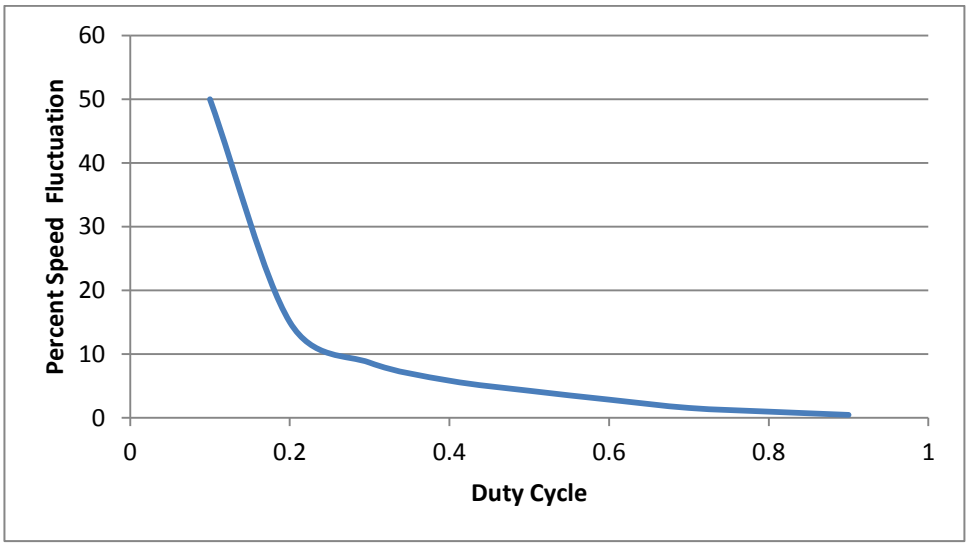

Figure 62 CA Speed fluctuation as a function of duty cycle

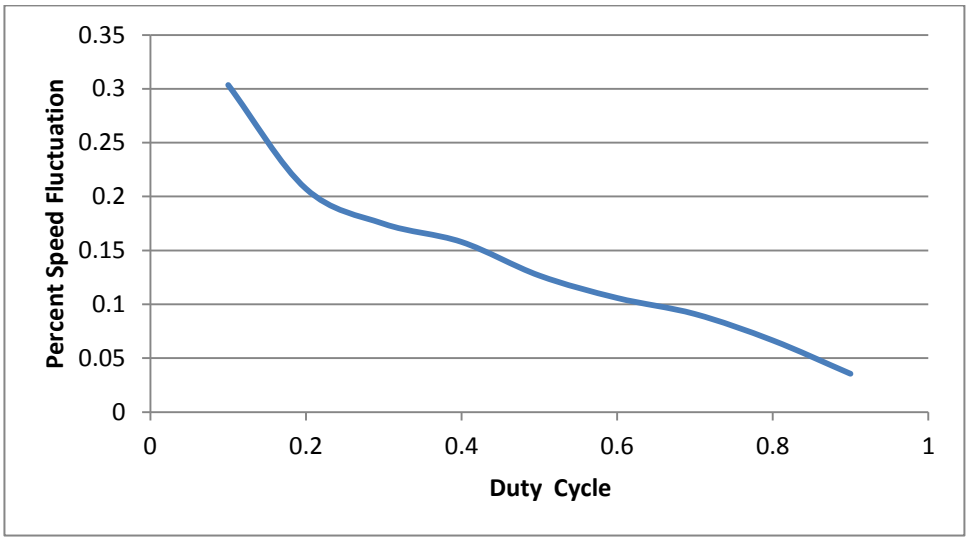

Figure 63 PWM speed fluctuation as a function of duty cycle

As it can be seen the area of operation for the proposed technique will heavily depend upon the acceptable speed fluctuations for a particular system, the simulations show how the fluctuations become excessive at low duty cycles for the propped technique whilst the more conventional PWM technique stays relatively steady independent of duty cycle.

9.2 Efficiency

Other Simulators model the ESC as an ideal device or only go as far as to take into account the on state resistance associated with the H-bridge resistance. Hence do not give results regarding switching losses. The steps outlined in chapter 7.4 allow are implemented in order to give results taking switching losses into account.

A suitable MOSFET has been selected, that has a maximum operating current and voltage of 20 V/1 A, as the motor draws a maximum current at stall of around 0.5 A. Relevant values can be seen in Table 13 where the specification sheet for the MOSFET is included within APPENDIX-B. A switching frequency of 32 kHz has been chosen for simulations involving efficiency and switching losses.

Table 13- Power MOSFET NTGS3441 relevant data

MOSFET Data	value	units
On state resistance	0.135	Ohms
Switch on time	70	ns
Switch off time	95	ns

This test compares the overall efficiency of the BLDC system depending upon current control technique. Figure 64 and Figure 65 show the switching losses for both PWM and Conduction Angle Control. Both strategies ran at 99 % duty cycle and torque was ramped up from zero to 0.5mNm [stall torque]over a period of ten second. Ramping up the load slowly in this way allows the time to be directly related to percent load, with ten seconds representing full load. As can be seen, the PWM switching losses are significantly greater [note the scalar on y axis] than those for the CA technique.

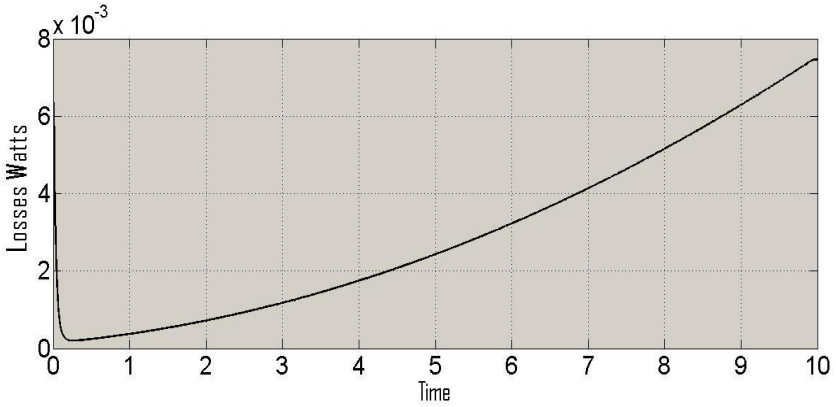

Figure 64 PWM switching losses vs load

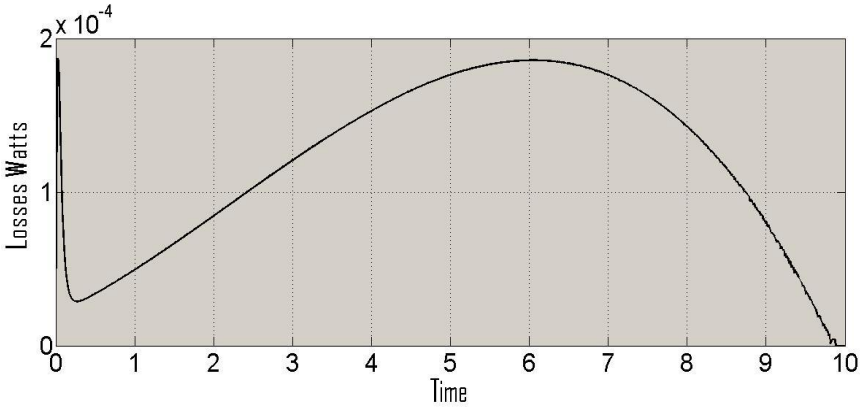

Figure 65 CA switching losses vs load

However switching losses are only one part of the losses for ESC, taking into account resistive losses for the same experiment put things into perspective. Figure 66 is the plot of total efficiency for the ESC for both techniques. This shows how resistive losses account for the majority of losses. Figure 67 is a plot detailing the increase in overall efficiency offered by the CA technique compared to conventional PWM. As can be seen when compared to other losses within the ESC the gain is minimal indeed, offering around a 0.3 % increase in a best case scenario.

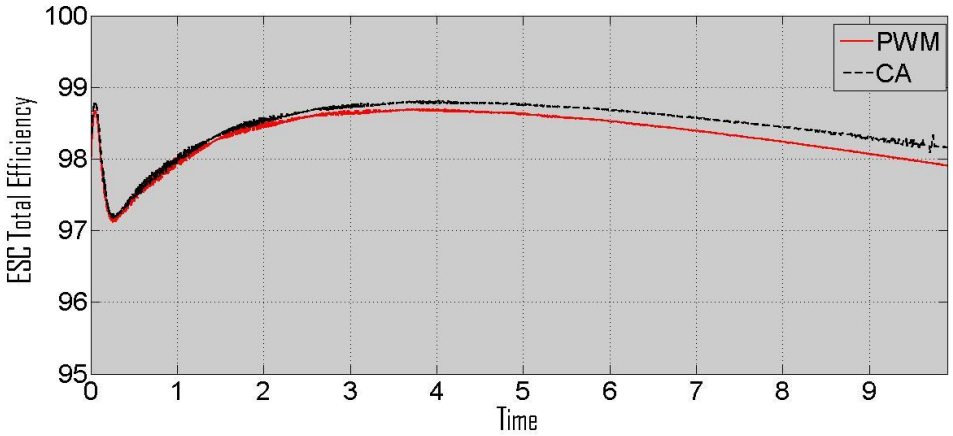

Figure 66 ESC efficiency

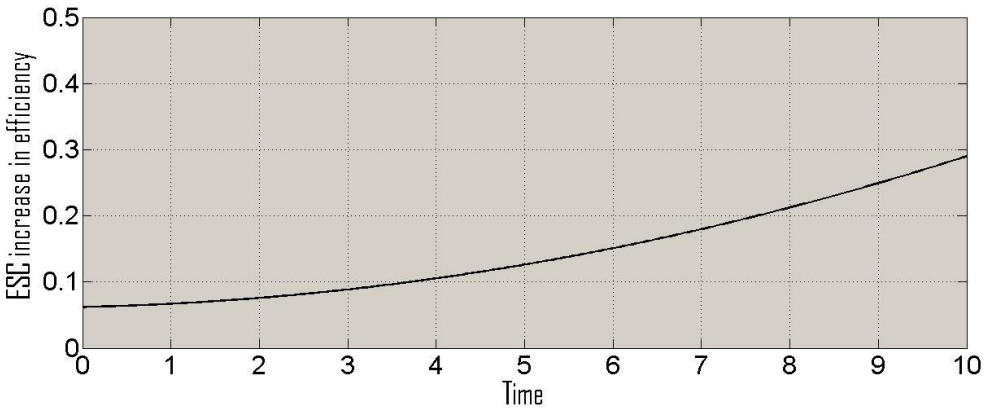

Figure 67 Percent increase for ESC efficiency

9.3 Locked Rotor

A locked rotor is a situation where the torque demanded from the motor is much greater than its stall torque, this leads to the rotor coming to a halt. This situation is quite common and usually arises from obstruction in the mechanical system, such as drive train failure. In the event of a situation like a conventional control technique would increase the duty cycle to 1 but as the rotor can't move to the next commutation step this higher than normal input current would run through the same high and low side switches in the H-brig indefinitely, leading to their imminent failure.

Due to the proposed power control technique being implemented using a time dependant input pulse, it should have inherent over current protection.

This is simulated by introducing a sudden load of sufficient magnitude to instantly lock the rotor, in this case a unit step input is used to introduce a load five magnitudes larger than the stall torque at a time of 0.05. Figure 68 shows that this situation does indeed lead to a locked rotor situation. By comparing Figure 69 and Figure 70 it can be seen that both techniques responded as expected, with the proposed technique cutting current and saving the components and PWM control showing no inherent safety against the same situation.

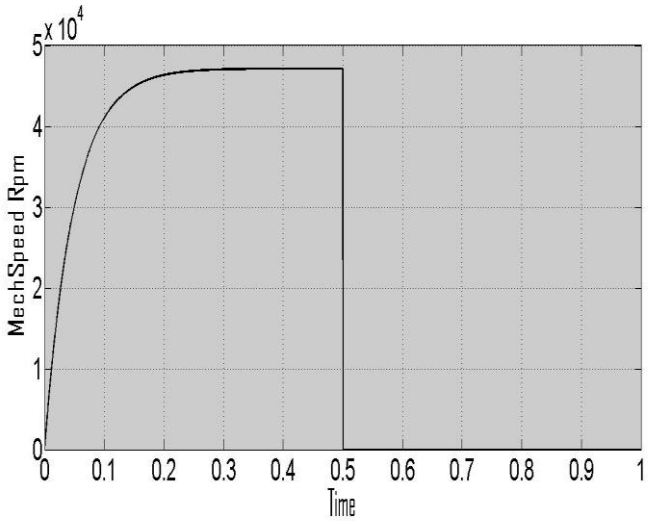

Figure 68 Speed response For simulated locked rotor situation

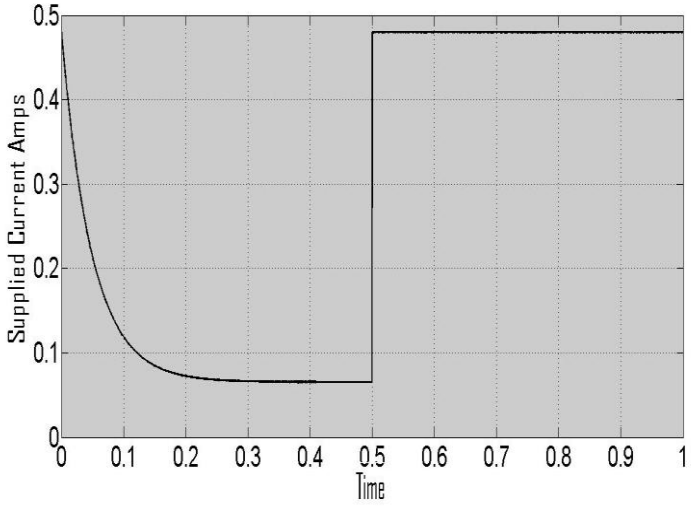

Figure 69 PWM current draw for locked rotor situation, Note prolonged high current

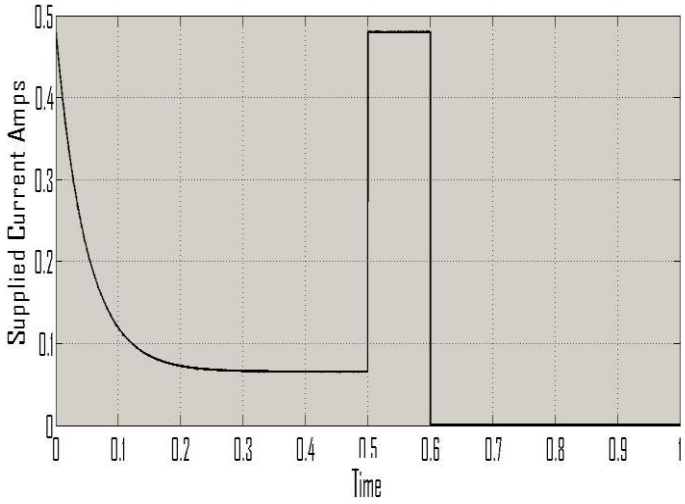

Figure 70 CA Current draw for locked rotor situation, Note current protection

9.4 Load Change and Stability

This Simulation set is aimed at checking the techniques robustness to changes in load that are within the systems operating range, that is changes in loads that are well below stalling torque. From the last chapter it is obvious that the minimum duty cycle is limited for the CA technique, taking this into consideration two conditions are simulated to test the robustness. The first changes the desired speed using unit step inputs from 4.5e4 rpm to 3e4 rpm applied at 0.1 seconds whilst operating under no load conditions, the second the ability of the control system to account for load changes by having a desired speed of 3e4 rpm initially unloaded and then its response to a unit step input mimicking a sudden increase of motor load at 0.1 seconds of 0.05 mNm [a quarter of its stall load].

Initially trial and error was used to verify the control loops operation, suitable values were found. Later the well known Zieger Nicholas Method of control loop tuning was tried, however for the common method it is required to increase proportional values until in the region between stable and unstable is reached [constant amplitude oscillations] however due to this system being inherently stable this was not practical or possible. Because an increase in system inertia would increase the inherent stability of the system, for the purpose of the following control simulations a worst case scenario is assumed. Modelling the inertia of the system as that of just the motor alone.

Control loop tuning is a large scientific field in itself and many other tuning techniques have been well established, of these many it seemed that a method named "Good Gain Method" which is a relatively simple experimental method that doesn't require oscillation of the system would suffice, [see APPENDIX-D] upon implementation the tuned parameters matched closely to those gained by trial and error.

The simulation results for stability when confronted with a change in desired speed or change in load are shown in Figure 71,Figure 72, Figure 73 and Figure 74 for CA and PWM respectably. Using the control values listen in Table 14. As can be seen CA reacts Just as well as PWM to both a moderate increase in load and change in set speed, further tests for the inverse of shown tests [sudden decrease of load and inverse change in set speed] follow the same trend of similarity.

Table 14 Control values for stability tests [Good Gain Method]

Control Values	CA	PWM
Kp	2.2e-5	2.2e-5
Ki	5e-3	5e-3
Kd	0	0

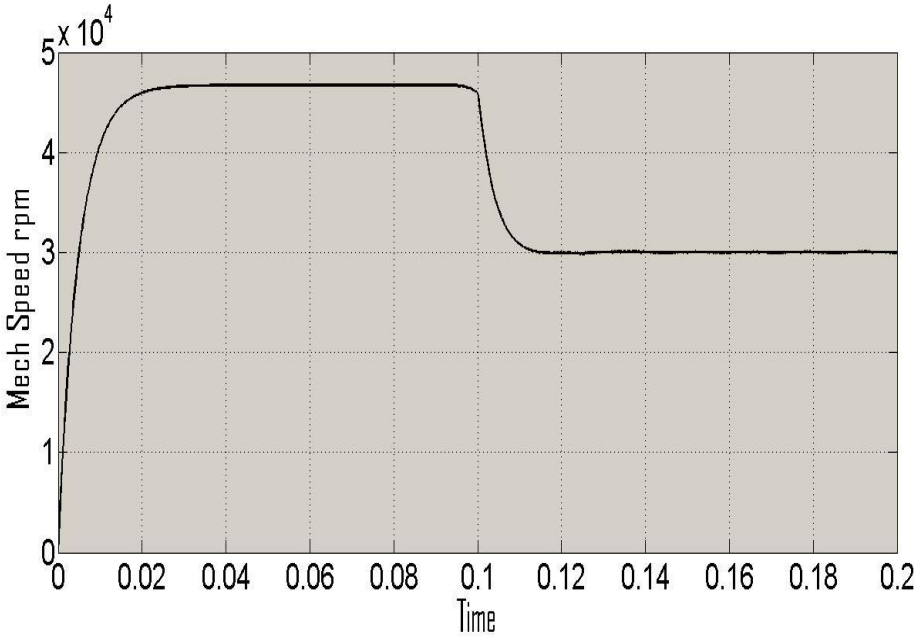

Figure 71 PWM reaction to decrease in set speed

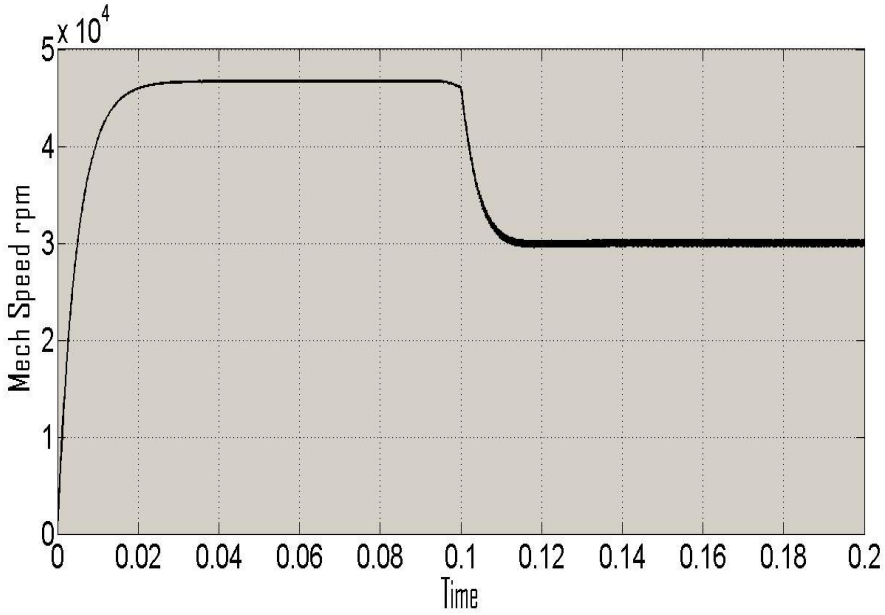

Figure 72 CA reaction to decrease in set speed

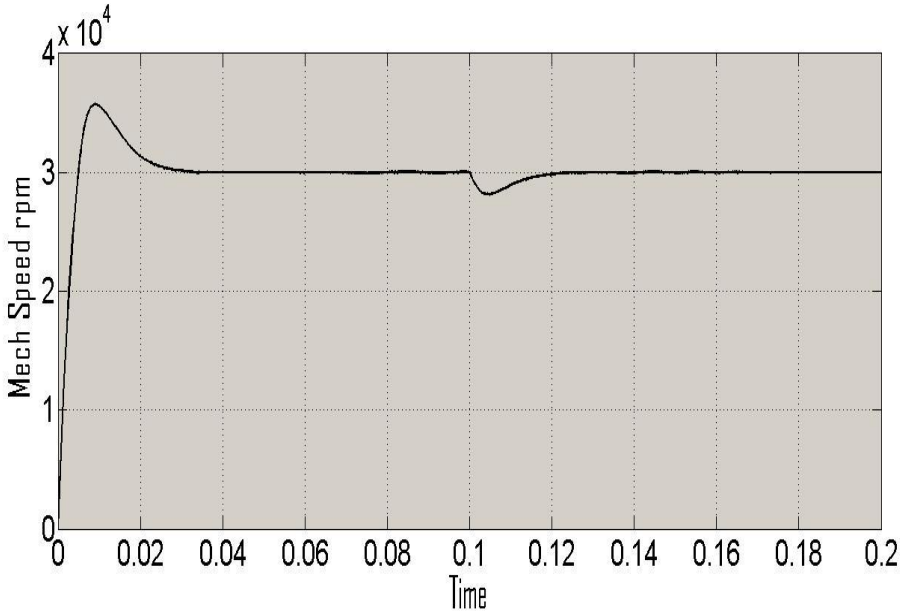

Figure 73 PWM reaction to increase in load

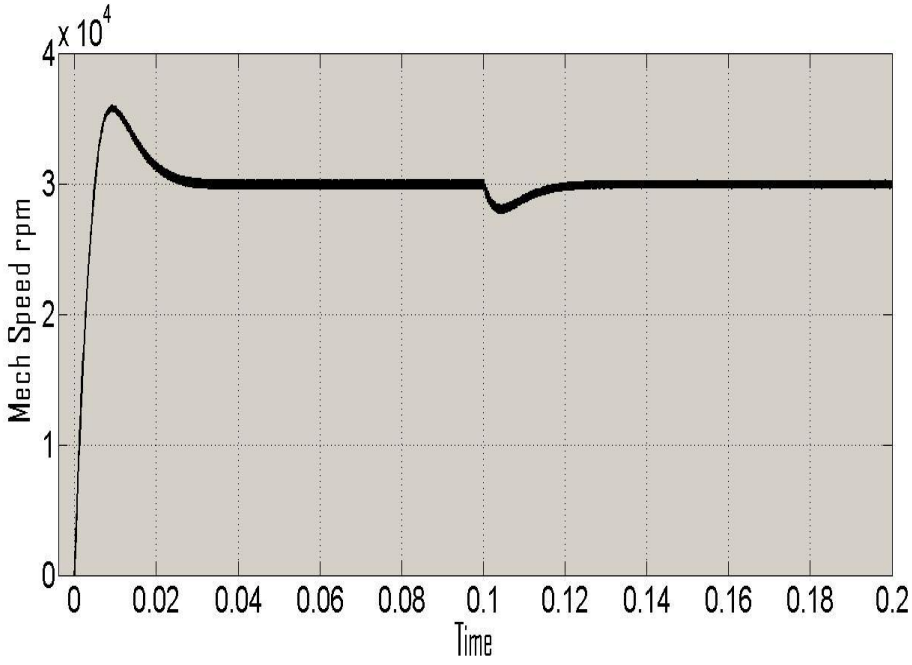

Figure 74 CA reaction to increase in load

Conclusions

In overview, the proposed CA commutation technique has been successfully simulated and results compared to those of traditional techniques, in this case PWM. Simulation results have successfully given numeric values for the increase of commutation efficiency, although an increase in efficiency can be achieved with the proposed technique when considering the magnitude of this increase; it is clear that it is only a small increase. In some energy critical systems, such as UAV [Unmanned Aerial Vehicles], where even small increases in efficiency are sought after, for example to increase flight time. However for many mainstream applications of moderately sized motors this increase will not offer enough of a benefit to warrant implementation due to the inherent speed fluctuations when operating at low duty cycles.

In smaller and budget systems that operate at a relatively high duty cycle such as many white goods, the increase in efficiency and reduction of complexity could offer benefits. It could also be of benefit to control very high speed motors, where extreme commutation frequencies don't allow for conventional PWM control as the PWM frequency must be higher than the commutation frequency. Simply be employed by varying the length of dead time between commutation steps, that is already present to prevent shoot through, where high side and low side switch on the same phase both being open simultaneously creating a short circuit.

The theory of inherent locked rotor protection was also tested, as expected the proposed technique does offer inherent protection that other systems lack. Many systems ignore the possible situation of locked rotor at the expense of mechanical problems leading to controller failure. In higher end quality systems this is avoided by adding additional sensing equipment to disable the controller if a problem is encountered in order to protect the semiconducting devices from premature failure.

Further Work

Further investigation and work regarding CA control would not be recommended unless for the purpose of a control system for a system with well-defined operating conditions that are known to work well with the CA technique, high duty cycle or inertia systems.

Building upon the Simulator and taking into account the losses associated with any reverse recovery diodes within the ESC, would give results of better quality. Furthermore this addition would allow the modelling of motors utilising regenerative breaking, this would be beneficial as this is another up and coming trend.

One of the large assumptions of this simulator is an ideal BEMF of a trapezoidal shape. This is rarely achieved in the real world due to manufacturing restraints. It is relatively simple to measure the real wold BEMF waveform. If the simulation software were to be modified to take this into account, much greater accuracy could be gained that would be useful in the fine tuning of control systems for reduced noise or efficiency.

The simulation taking into account losses takes considerable time to produce results. This is mainly because of the way PWM waveforms are generated and, the high tolerance related to this portion of the simulator. The abundance of scopes dotted around saving background data used in the building of the sub blocks. Removing any unneeded scope blocks and a redesigned PWM generator would be beneficial before any large strings of simulations are ran.

References

1. **George Gulalo** *Motion Tech Trend***s.** *Electric Motor Market in North America, 2002 & 2007.*

2. **Paul Walde, Conrad u. Brunner.** *Energy-Efficiency Policy Opportunities for Electric Motor-Driven Systems.* s.l. : InternatIonal energy agency, 2011.

3. **Yedamale, Padmaraja.** Brushless DC (BLDC) Motor Fundamentals. 2003. Vol. http://electrathonoftampabay.org/www/Documents/Motors/Brushless%20DC%20%28BLDC%29%20Motor%20Fundamentals.pdf.

4. **Yedamale, Padamara ja.** *Brushless DC (BLDC) MotorFundementals Microchip Technology inc.* 2003.

5. **Stefan Baldursson.** *BLDC Motor Modeling and Control - A MATLAB/SIMULINK Implimentation.* 2005.

6. **James robert Mavey.** *Sensorless field oriented control of brushless permanent magnet synchronous motors.* s.l. : Kansas State University, 2006.

7. **Lee, Shiyoung.** *"Evaluation of a software configurable digital controller for the permanent magnet synchronous motor using field-oriented control.* s.l. : in SSST system theory, 2010, pp. 302-306.

8. **T. W Ching,.** *Soft-switching Converters for Electric Vehicle Propulsion.* s.l. : Journal of asian electric vehicles vol. 5, no. 2, pp. 1019-1026, 2007.

9. **Tom Lemley, Shiyoung Lee.** A comparison study of the commutation methods for the three-phase permenent magnet brushless motor. *http://www.magnelab.com/uploads/4c51d9ba6fe5a.pdf.* [Online] [Cited: 04 04 2013.]

10. **Han Woong Park, Man Hyung Lee, Fumio Harashima Sung Jun Park.** *A new approach for minimum-torque-ripple maximum-efficiency control of BLDC motor.* s.l. : IEEE Industrial electronics, vol. 47, no. 1, pp. 109-114, feb 2000.

11. **Vineeta Gangla Tomy Sebastian.** *Analysis of induced EMF waveforms and torque ripple in a brushless permanent magnet machine.* s.l. : IEEE Industrial aplications, vol. 32, no. 1, pp. 195-200, Feb 1996.

12. **Yedamale, Padmaraja.** *rushless DC (BLDC) motor fundamentals.* s.l. : microchip technology inc, 2003.

13. **Bon-Gwan Gu, Jin-Hong Kim,Jun-Hyuk Choi,In-Soung Jung Joon Sung Park.** *Development of BLDC motor drive for automotive.* s.l. : aaplications ESARS electrical systems for aircraft, railway and ship propulsion, 2012, pp. 1-6.

14. **Z. Q. Zhu, David Howe Yong Liu,.** *Direct torque control of brushless DC drives with reduced torque ripple.* s.l. : IEE industrial aplications confrence, vol. 4, pp. 2390-2396, Oct 2004.

15. **Texax Instruments.** *Field orientated control of 3-phase AC-motors.* s.l. : BPRA073, 1998.

16. **Sundaram, Meenakshi.** *Implementing field oriented control of a brushless DC motor.* s.l. : Cypress Semiconductor , (01/04/2012).

17. **K.T.Chan.** *Overview of permanent magnet brushless drives for electric and hybrid electric vehicles .* s.l. : IEEE Transaction on industrial electronics, no. 6, pp. 2246-2257, June 2008.

18. **Volodymy Ivakhno r.** *Estimation of Semiconductor Switching Losses under Hard Switching using Matlab/Simulink Subsystems.* s.l. : Electrical, Control and Communication Engineering. Volume 2, Issue 1, Pages 20–26, ISSN (Online) 2255-9159, ISSN (Print) 2255-9140, DOI:, 2013.

19. **Ernesto Vázquez-Sánchez, Jaime Gómez-Gil Gamazo-Real José Carlos.** *Position and speed control of brushless DC motors using sensorless techniques and application trends .* s.l. : ISSN 1424-8220, pp. 6901-6947, 20120.

20. **Bojan Gr˘car, Peter Cafuta, Gorazd Stumberger Aleksandar M. Stankovi´c,.** *Pulsating torque reduction for permanent magnet AC motors.* s.l. : IEEE control aplications, 2001, pp. 288-293.

21. **Evans, D. Brown P. D.** *Simulation of Low Voltage Brushless DC Motr Drives.* s.l. : University of Bath.

22. **Mohammad Sharokhi, Alireza Zomorrodi.** *Comparison of PID controller Tuning Methods.* s.l. : 8th National Iranian Chemical Engineering Congress.

23. **P. Andrada, M.Torrent, J.I.Perat, B. Blanqué.** *Power Losses in Outside-Spin Brushless D.C. Motors.*

24. **Shiyoung Lee, Ph.D.** *A COMPARISON STUDY OF THE COMMUTATION METHODS.* http://www.magnelab.com/uploads/4c51d9ba6fe5a.pdf.

25. **Mavey, James robert.** *Sensorless field oriented control of brushless permanent magnet synchronous motors.* s.l. : B.S., Kansas State University, 2006.

26. **Syed A. Hossain, Pedro Reis.** *Effect of BLDC Motor Commutation Schemes on Invertoer Power Loss.* s.l. : IEEE Electric Machines Paper ID 1339, 2008.

27. **Article, Copley Controls Corp.-.** What is ‘Field Oriented Control’ and what good is it? s.l. : http://www.maccon.de/fileadmin/FTPROOT/Field-Oriented-Control.pdf, Visited 04/04/13.

Appendix A

Motor Data Sheet

Appendix B

Mosfet Data Sheet

Appendix C

BEMF Code

The following code is an example of the style used throughout the simulator in where code allowed a quicker or precise alternative to block diagram implementation. The code below takes into account motor constants, speed and angular position to generate estimates of the BEMF produced by the motor at that instance. Input u1 provides the position of the rotor and calculates the BEMF for each phase [y1,y2,y3 being a,b,c respectably] based the total BEMF that is calculated using block diagram methods and fed into the code as input u2.

```
%{ Michael Thomas Ratcliffe m.ratcliife@lancaster.ac.uk

 This program is free software: you can redistribute it and/or
modify it under the terms of the GNU General Public License as
published by the Free Software Foundation, either version 3 of
the License, or(at your option) any later version. This program
is distributed in the hope that it will be useful but WITHOUT
ANY WARRANTY; without even the implied warranty of
MERCHANTABILITY or FITNESS FOR A PARTICULAR PURPOSE.  See the
GNU General Public License for more details:

<http://www.gnu.org/licenses/>. %}



function [y1,y2,y3] = BEMF(u1,u2) %%Declaring inputs and
outputs

    if 0<=u1 && u1<60           y1=u2; %%Top of trapezoid
      y3=(((6*u2)/180)*(60-(u1)))-u2;
      y2=-u2;

    else if 60<=u1 && u1<120
y1=u2;
y3=-u2;
y2=((((6*u2)/180))*((u1)-(120)))+u2;

    else if 120<=u1 && u1<180
y1=(((6*u2)/180)*(180-(u1)))-u2;
y3=-u2;
y2=u2;


    else if 180<=u1 && u1<240
y1=-u2;
y3=((((6*u2)/180))*((u1)-(240)))+u2;
y2=u2;


    else if 240<=u1 && u1<300
y1=-u2;
```

```
y3=u2;
y2=(((6*u2)/180)*(300-(u1)))-u2;



    else if 300<=u1 && u1<361
y1=((((6*u2)/180))*((u1)-(360)))+u2;
y3=u2;
y2=-u2;


  else           %% This statement is included for error
checking
y1=1000000000;
y2=1000000000;
y3=1000000000;

        end
        end
        end
        end
        end


    end
```

Appendix D

Good Gain PID Tuning Theory

Appendix E

Input Variables for Final Tests

All variables assigned as below with CA and PWM being assigned a high value to activate the desired simulation.

Note: variables that do not effect simulation marked NA

Section 9.1 Simulation Inputs

Vs	6	
R	6.25	
L	0.0455e-3	
Kv	1.05e-3	
J	5e-9	
Fr	1.38e-8	
P	2	
H_Rt	0	
H_Toffon	0	
H_Freq	32000	
LoopFreq	1000	
P_Toffon	0	NA
P_Rt	0	NA
P_Freq	0	NA
Kp	2.2e-5	NA
Ki	5e-3	NA
Kd	0	NA
PWM	0	
PAM	0	
CA	0	

Section 9.2 Simulation Inputs

Vs	6
R	6.25
L	0.0455e-3
Kv	1.05e-3
J	5e-9
Fr	1.38e-8
P	2
H_Rt	0.117
H_Toffon	165e-9
H_Freq	32000
LoopFreq	1000
P_Toffon	0
P_Rt	0
P_Freq	0
Kp	2.2e-5
Ki	5e-3
Kd	0
PWM	0
PAM	0
CA	0

Section 9.3 Simulation Inputs

Vs	6	
R	6.25	
L	0.0455e-3	
Kv	1.05e-3	
J	5e-9	
Fr	1.38e-8	
P	2	
H_Rt	0	NA
H_Toffon	0	NA
H_Freq	32000	
LoopFreq	1000	
P_Toffon	0	NA
P_Rt	0	NA
P_Freq	0	NA
Kp	2.2e-5	NA
Ki	5e-3	NA
Kd	0	NA
PWM	0	
PAM	0	
CA	0	

Section 9.4 Simulation Inputs

Vs	6	
R	6.25	
L	0.0455e-3	
Kv	1.05e-3	
J	5e-10	
Fr	1.38e-8	
P	2	
H_Rt	0.117	
H_Toffon	165e-9	
H_Freq	32000	
LoopFreq	1000	
P_Toffon	0	NA
P_Rt	0	NA
P_Freq	0	NA
Kp	2.2e-5	
Ki	5e-3	
Kd	0	
PWM	0	
PAM	0	
CA	0	

Appendix F

Published in:

Power Engineering, Energy and Electrical Drives (POWERENG), 2013 Fourth International Conference

Date of Conference:

13-17 May 2013

Page(s):

1700 - 1705

ISSN :

2155-5516

INSPEC Accession Number:

13860857

Conference Location :

ISTANBUL